Ocean Mesoscale and Frontal-scale Ocean-Atmosphere Interactions and Influence on Large-scale Climate: A Review

US CLIVAR Mesoscale Air-Sea Interaction Working Group

Hyodae Seo* (Woods Hole Oceanographic Institution, Woods Hole, MA, USA)
Larry W. O'Neill (Oregon State University, Corvallis, OR, USA)
Mark A. Bourassa (Florida State University, Tallahassee, FL, USA)
Arnaud Czaja (Imperial College London, London, United Kingdom)
Kyla Drushka (Applied Physics Laboratory, University of Washington, Seattle, WA, USA)
James B. Edson (Woods Hole Oceanographic Institution, Woods Hole, MA, USA)
Baylor Fox-Kemper (Brown University, Providence, RI, USA)
Ivy Frenger (GEOMAR Helmholtz Centre for Ocean Research Kiel, Germany)
Sarah T. Gille (Scripps Institution of Oceanography, University of California San Diego, La Jolla, CA, USA)
Benjamin P. Kirtman (University of Miami, Miami, FL, USA)
Shoshiro Minobe (Hokkaido University, Sapporo, Japan)
Angeline G. Pendergrass (Cornell University, Ithaca, NY, USA)
Lionel Renault (LEGOS, University of Toulouse, Toulouse, France; Atmospheric and Oceanic Sciences, University of California, Los Angeles, CA, USA)
Malcolm J. Roberts (Met Office Hadley Centre, Exeter, United Kingdom)
Niklas Schneider (University of Hawai'i at Manoa, Honolulu, HI, USA)
R. Justin Small (National Center for Atmospheric Research, Boulder, CO, USA)
Ad Stoffelen (Royal Netherlands Meteorological Institute, Utrecht, the Netherlands)
Qing Wang (Naval Postgraduate School, Monterey, CA, USA)

Submitted to J. Climate

*Corresponding author: Hyodae Seo (hseo@whoi.edu)

Abstract

Two decades of high-resolution satellite observations and climate modeling studies have indicated strong ocean-atmosphere coupled feedbacks mediated by small-scale oceanic processes, including semi-permanent and meandrous SST fronts, mesoscale eddies, and filaments. The air-sea exchanges in latent heat, sensible heat, momentum, and carbon dioxide associated with this so-called mesoscale air-sea interaction are found robust near the major western boundary currents, Southern Ocean fronts, equatorial and coastal upwelling zones, but they are also ubiquitous over the global oceans wherever ocean mesoscale processes are active. Current theories, informed by rapidly advancing observational and modeling capabilities, have established the importance of mesoscale air-sea interaction processes for understanding large-scale ocean circulation, biogeochemistry, and weather and climate variability. However, numerous challenges remain to diagnose, observe, and simulate mesoscale air-sea interaction accurately to quantify its impacts on large-scale processes. This article provides a comprehensive review of investigations of many key aspects pertinent to mesoscale air-sea interaction, synthesizes current understanding with remaining gaps and uncertainties, and provides recommendations on theoretical, observational, and modeling strategies for future air-sea interaction research.

Significance Statement

Recent high-resolution satellite observations and climate models have characterized coupled ocean-atmosphere interactions mediated by small-scale (mesoscale) ocean processes, including ocean eddies and fronts. Ocean mesoscale-induced spatial temperature and current variability modulate the air-sea exchanges in heat, momentum, and mass (e.g., gases such as carbon dioxide and water vapor), altering coupled boundary layer processes. Studies suggest that skillful simulations and predictions of ocean circulation, biogeochemistry, and weather and climate events depend on accurate representation of the eddy-mediated air-sea interaction. However, numerous challenges remain to diagnose, observe, and simulate mesoscale air-sea interaction accurately to quantify its large-scale impacts. This article synthesizes the latest understanding of mesoscale air-sea interaction, identifies remaining gaps and uncertainties, and provides recommendations on strategies for future ocean-weather-climate research.

1. Introduction

Decades of observational and modeling analysis have broadly identified two fundamental regimes of ocean-atmosphere coupling that are dependent on the spatial scale of ocean surface variability. The first regime involves the ocean response to large-scale (>1000 km) atmospheric internal variability, which drives a response in sea surface temperature (SST) through the mediation of surface turbulent heat fluxes and upper-ocean turbulent mixing (e.g., Frankignoul et al. 1985; Alexander and Scott 1997). The large-scale ocean response feeds back onto the incipient atmospheric circulation anomaly to either reinforce or erode it (e.g., Bladé 1997). In this framework, the ocean is viewed as relatively passive, mainly advecting anomalies, storing heat, and serving as a source of noise forcing.

The second regime, the focus of this paper, involves an atmospheric response driven by mesoscale eddy-induced spatial SST and current variability. Here, the term "mesoscale eddies and fronts" broadly refers to all forms of oceanic processes with horizontal length-scales smaller than the first regime of air-sea interaction (>1000 km) but larger than oceanic submesoscale (~10 km). These processes include coherent, swirling, and transient ocean circulations with length-scales near the Rossby radius of deformation (Chelton et al. 2011), filamentary eddy structures that are widely observed in coastal upwelling systems, and semi-permanent fronts and undulations near the midlatitude western boundary currents (WBCs) and their extensions, and SST fronts along the equatorial tongue in the Pacific and Atlantic oceans.

The SST signature from these ocean mesoscale processes modifies surface turbulent heat and momentum fluxes, driving local responses in marine atmospheric boundary layer (MABL; e.g., Small et al. 2008), while MABL responses drive non-local responses in the path and activity of storm tracks in the extratropics (e.g., Czaja et al. 2019) and deep moist convection in the tropics (e.g., Li and Carbone 2012; Skyllingstad et al. 2019; de Szoeke and Maloney 2020). The atmospheric response to ocean mesoscales feeds back onto eddy activity and SST, and alters the large-scale ocean circulation, further influencing these atmospheric processes (e.g., Nakamura et al. 2008; Hogg et al. 2009; Frankignoul et al. 2011; Taguchi et al. 2012). The surface currents from the ocean mesoscale eddies also affect the wind stress and heat fluxes as well as the wind profiles in the MABL, which influence ocean circulation, including the stability and strength of

the WBCs (Renault et al. 2016b, 2019b) and the basin-scale coupled climate variability such as ENSO (e.g., Luo et al. 2005). Ocean forcing of the atmosphere increases with time-scale and decreases with increasing spatial scale (Bishop et al. 2017), suggesting the need to include mesoscale eddies in coupled climate model simulations (e.g., Bryan et al. 2010; Kirtman et al. 2012; Roberts et al. 2016).

Aside from earlier limited observational studies showing the synoptic evidence of MABL response to mesoscale SSTs (e.g., Sweet et al. 1981), the first global-scale surveys of the MABL and surface wind responses were provided by Chelton et al. (2004) and Xie (2004), followed by a comprehensive review paper by Small et al. (2008) and Kelly et al. (2010). The number of publications that include aspects of mesoscale air-sea interaction has grown exponentially in the last decade (See Robinson et al. 2018, 2020), which also emphasizes a strong cross-disciplinary nature of the research subject, encompassing nearly all fields of atmospheric, oceanographic, and climate sciences using theories, observations, and modeling (e.g., AMS Special Collection on *Climate Implications of Frontal Scale Air-Sea Interaction*, and the *J. Oceanography* Special Collection on "Hot Spots" in the climate system, Nakamura et al. 2015). This review paper will provide a synthesis of the latest advances in process-understanding from these investigations, mainly focusing on work done in the last decade or so.

The paper is organized in the following way. The air-sea flux responses to mesoscale SST and surface currents are discussed in Section 2, along with theories and analytical studies of MABL dynamics describing the flux responses. Section 3 reviews the deep tropospheric responses, emphasizing the modulation of local and downstream adjustments of extratropical weather systems and their aspects related to climate change. Section 4 discusses thermal and mechanical feedback effects on ocean circulation and biogeochemistry, and also explores theories and parameterizations to account for eddy-atmosphere interaction. Section 5 discusses the emerging observational platforms to enable accurate measurements of air-sea interaction at small spatial scales. Section 6 provides a summary and discussion.

2. Boundary layer and surface heat, momentum, and gas flux responses

Surface fluxes communicate mass and energy between the ocean and atmosphere and are thus key processes in Earth's climate system. The ocean is a major reservoir of heat and carbon in the Earth system, and it is becoming increasingly clear that exchanges with the atmosphere occurring on the oceanic mesoscale are significant in shaping Earth's climate. Recent assessments on projected trends in surface air temperature (SAT) and SST have indicated a need to better understand surface heat fluxes in part to reconcile conflicting lines of evidence on the projected trends in SAT and SST (Box TS.1, IPCC 2021). The turbulent heat fluxes are composed of sensible and latent heat fluxes, while the surface wind stress represents the turbulent momentum flux between the atmosphere and ocean. This section discusses air-sea heat, momentum, and gas flux responses to spatially heterogeneous fields of SST, surface currents, and sea state. We also discuss the local MABL response to ocean-induced mesoscale forcing given its strong relationship with the surface fluxes.

Surface flux response to spatially heterogeneous SST and currents generates responses initially confined to the atmospheric and oceanic boundary layers, but feedbacks transfer the responses of this coupling to the free atmosphere above (Section 3) and the ocean thermocline below (Section 4). Figure 1 shows the strong correlation between monthly mesoscale surface fluxes and ocean mesoscale variability from the ERA5 reanalysis (Hersbach et al. 2020). When the local point-by-point correlation correlations between the fluxes are strongly negative (with the sign convention that the heat flux is positive downward), the SST variability can be viewed as the ocean forcing the atmosphere. Similarly, when the correlation between turbulent heat flux and SST *tendency* is negative, the atmosphere is viewed as driving ocean variability. Over mesoscale, the wind stress and upward heat fluxes are enhanced over warm spatial SST anomalies (SSTA) and reduced over cool SSTA. The correlations are much stronger for sensible and latent heat flux responses, while the surface stress response on this spatial scale is much more apparent in oceanic frontal boundary regions.

a. Turbulent heat flux response

On smaller scales encompassed by the oceanic mesoscale and time-scales longer than synoptic time-scales, spatial variations in surface turbulent heat flux are driven primarily by spatial

perturbations of SST, such that positive heat flux anomalies (i.e., ocean heat loss) occur over warm SST perturbations and negative heat flux anomalies (i.e., ocean heat gain) occur over cool SST perturbations (Figure 1). Over these scales, the ocean forces a response of the atmosphere driven by the surface heat exchange, which is fundamentally different from what occurs over larger spatial scales. Near-surface air temperature and specific humidity adjust slowly to spatially heterogeneous SST as air flows across SST fronts. Ocean mesoscale features and semi-permanent WBCs often generate large air-sea temperature and humidity differences. The most dramatic example was observed during the CLIMODE experiment near the Gulf Stream during wintertime, when air-sea temperature differences exceeded 10°C over 200 km, yielding >1000 W/m^2 surface turbulent heat fluxes into the atmosphere (Marshall et al. 2009).

Past field experiments captured less extreme but nonetheless strong responses of turbulent heat fluxes and MABL convective turbulence to mesoscale and frontal-scale SSTs. Examples can be found from the Sargasso Sea during the FASINEX experiment (e.g., Friehe et al. 1991), Gulf Stream (e.g., Plagge et al. 2016), Kuroshio (e.g., Tokinaga et al. 2009); Tropical Instability Waves (Thum et al. 2002), Brazil-Malvinas Confluence system (e.g., Pezzi et al. 2005; Villas Bôas et al. 2015; Souza et al. 2021), the Agulhas Current (e.g., Jury and Courtney 1991; Messager and Swart 2016), the western Arabian Sea (e.g., Vecchi et al. 2004).

The scale dependence has been quantified primarily from reanalysis-based surface flux and SST datasets (e.g., Li et al. 2017; Sun and Wu 2021). Bishop et al. (2017), in particular, show that on time-scales longer than one month, the turbulent heat fluxes on the oceanic mesoscale and frontal scale are driven by SST variability associated with oceanic internal processes. On shorter time-scales, the variability is driven more by synoptic-scale weather variability, particularly along the storm tracks overlying the WBCs. Based on this simple diagnostic, Kirtman et al. (2012) concluded that eddy-parameterized models grossly underestimate the ocean forcing of the atmosphere in eddy-rich regions (i.e., WBCs and the Southern Ocean) and overestimate the atmospheric forcing of the ocean throughout much of the mid-latitudes compared to the ocean eddy-resolving simulations.

b. Turbulent momentum flux and MABL wind responses

The turbulent heat flux response to SST is a key process that drives the responses in turbulent momentum flux to SST. The strong variability in ocean surface currents at mesoscales also affect the wind stress through the relative motion of the surface winds and currents. The most immediate local atmospheric response to SST and surface currents is initially confined to the MABL. The wind and wind stress responses mainly result from a dynamical adjustment of the MABL pressure and vertical turbulent stress profile distinct from simple adjustments of the surface layer logarithmic wind profile (e.g., Small et al. 2008; O'Neill 2012; Renault et al. 2016a).

1) Mesoscale SST effects

Traditionally, local atmospheric responses to the mesoscale SST have been characterized by empirical linear regressions between collocated mesoscale SSTs and surface winds and surface wind stress, all spatially high-pass filtered to isolate the coupling on scales smaller than about *O*(1000 km). Regression coefficients, called coupling coefficients, obtained from satellite-observed wind speed and wind stress show ubiquitous increases of their magnitudes over warm SSTs, increases of wind divergence and wind stress divergence co-located with the downwind component of SST, and wind curl and wind stress curl that scale with crosswind components of SST gradients (Chelton et al. 2001; O'Neill et al. 2003, 2012). The SST-induced curl and divergence responses provide further constraints on spatial scales of the SST-induced MABL response. These simple but powerful diagnostic metrics have helped to illuminate the simulated air-sea interaction over a range of scales in numerical models (Bellucci et al. 2021), leading to refinements in the SST resolution (Chelton 2005) and the PBL parameterizations in NWP models (Song et al. 2017). However, in this approach, the wind responses to SST include contributions from broad scales represented in high-pass filtered input fields. Alternative diagnostic approaches exist, including cross-spectral analysis (e.g., Small et al. 2005b; O'Neill et al. 2012; Laurindo et al. 2019; Samelson et al. 2020), cross-covariance and correlation functions between SST (and its tendency), and wind and turbulent heat fluxes (e.g., Frankignoul and Hasselmann 1977; Wu et al. 2006; Bishop et al. 2017; Small et al. 2019).

2) Mesoscale current effects

Regions of strong SST gradients are also regions of strong variability in ocean surface current. The current feedback (CFB) mechanism directly modifies wind stress through the relative motion of surface winds and currents, which in turn alters the low-level wind shear and wind: a negative current anomaly induces a positive stress anomaly, which in turn causes a negative wind anomaly (Renault et al. 2016a). At the mesoscale, CFB primarily impacts the surface wind stress curl but not its divergence due to the quasi-geostrophic nature of ocean currents (Chelton et al. 2004). The wind stress and wind responses to CFB can be also diagnosed using empirical relationships based on satellite and numerical simulations. Renault et al. (2016a; 2019a) defined two coupling coefficients related to CFB: s_w is the slope of the regression between mesoscale surface currents and 10 m wind and s_τ is the linear regression coefficient linking mesoscale surface current and surface stress. The coefficient s_τ can be interpreted as a measure of the CFB efficiency: the more negative s_τ, the more efficient an eddy killing. The effect on the ocean is discussed in detail in Section 4.

The SST and current-induced stress responses are challenging to separate since mesoscale SST and current variations tend to co-vary strongly near ocean fronts and eddies. Nonetheless, estimates of the contributions of the current-induced wind stress response via the linear coupling coefficients indicate that the current-induced stress anomalies exceed the SST-induced response over strong WBCs and within isolated ocean eddies (e.g., Gaube et al. 2015; Renault et al. 2019a). The current-induced stress response exists in scatterometer and direct air-sea flux observations and coupled ocean-atmosphere simulations but is not directly apparent in atmosphere-only simulations and reanalyses, such as the ERA5 wind stress anomalies used in Figure 1. Including both current and SST-induced stress anomalies has a particularly strong impact on the mesoscale wind stress curl field.

c. Analytic framework for SST-induced boundary layer response

The MABL response to ocean mesoscale current must incorporate coupling between the MABL thermodynamics and dynamics to adequately represent the influence of SST and surface current on the surface wind stress and sensible and latent heat fluxes. An analytical framework for SST impacts was recently proposed, which incorporates MABL heat and momentum budgets that

capture the first-order response of the MABL to SST forcing (Schneider and Qiu 2015; Schneider 2020) and includes representation of the processes shown in the literature to be of primary importance. This framework considers an MABL capped by an inversion (Battisti et al. 1999). Within this layer, air temperature is assumed well mixed and vertically constant and subject to horizontal advection and air-sea heat exchanges. The system is driven by winds with horizontal scales far larger than the ocean mesoscale that satisfy a drag law at the sea surface and experiences zero vertical momentum flux at the inversion. The large-scale winds $\vec{U}$ form a modified Ekman spiral (Holton 1965a,b), which is considered horizontally homogeneous on scales commensurate with the ocean mesoscale.

SST T enters the heat budget of the layer via the air-sea heat exchanges due to the air-sea temperature difference with rate γ. Air temperature Θ results to first order from a steady balance of surface sensible heat fluxes with advection by large-scale winds (e.g., Small et al. 2005a),

$$\vec{U} \cdot \nabla\Theta = \gamma(T - \Theta),$$

The MABL air temperatures Θ adjust to T over a length-scale of U/γ, forming a wake of elevated values of the air-sea temperature differences in the lee of spatial SST variations. Thermal adjustment rates of the boundary layer γcorrespond to adjustment times of the order of a few hours to half a day (Schubertet al. 1979), yielding length scales of *O*(100 km). The momentum equations govern the wind response to the ocean mesoscale SST-induced acceleration $\vec{F}$,

$$\vec{U} \cdot \nabla\vec{u} + \frac{w^\star}{H}\partial_s\vec{U} + f\hat{e_3} \times \vec{u} - \frac{1}{H^2}\partial_s A \partial_s \vec{u} + g'\nabla h = \vec{F},$$

which include on the lhs horizontal advection by large-scale winds $\vec{U}$ of SST induced winds $\vec{u}$ and vertical advection $w^\star$ of the large-scale shear, the Coriolis acceleration with Coriolis frequency f, the divergence of vertical fluxes of horizontal momentum due to large-scale mixing with eddy coefficient A, and hydrostatic pressure gradient forces, including the so-called back pressure effect (e.g., Hashizume et al. 2002) due to ocean mesoscale-induced changes of inversion height h. Together with the continuity equation and boundary conditions of a drag law

at the sea surface, and a material inversion with no flux of momentum, these equations provide a complete analytical solution for the wind response to ocean mesoscale SSTs.

Changes of Θ impact accelerations $\vec{F}$ to the horizontal momentum on the rhs through the hydrostatic pressure term, which couples the MABL thermodynamics with the dynamics:

$$\vec{F} = \frac{gH}{\Theta_0}(1-s)\nabla\Theta + \frac{1}{H^2}\partial_s\left(\dot{A}\,\partial_s\vec{U}\right) \quad (1)$$

through the modulation of the hydrostatic pressure gradients (the first term on the right), and the sensitivity of the vertical mixing to the fluxes at the air-sea interface (the second term on the right). The sigma vertical coordinate s measures the height relative to the mean inversion height H, Θ_0 is a reference temperature, g the earth's gravitational acceleration, and $\dot{A}$ is the sensitivity of vertical mixing A to SST.

The vertical mixing effect, the second term on the right on Eq. (1), is a linearization of the 'nonlinear' term envisioned by Wallace et al. (1989) and Hayes et al. (1989) that captures the modulations of the vertical mixing acting on the large-scale wind profile. The dynamics, amplitude, and vertical structure of $\dot{A}$ determine the character of mixing sensitivity. Mixing can intensify and change its vertical scale. The dependence of vertical mixing on the non-equilibrium air-sea temperature difference is but one possibility. Alternatively, SST induces convective adjustment of the lapse rate and permanently deepens the boundary layer over warmer waters (Samelson et al. 2006). These diagnostic formulations for $\dot{A}$ are endpoints of the non-equilibrium evolution of vertical mixing simulated by LES (e.g., de Szoeke and Bretherton 2004; Skyllingstad et al. 2007; Sullivan et al. 2020), which allow for changes of the vertical mixing that lag modulations of boundary layer stability (Wenegrat and Arthur 2018). As such, the coupling between surface winds and SST is sensitive to the MABL turbulence closure schemes (e.g., Song et al. 2009, 2017; Perlin et al. 2014; Samelson et al. 2020).

Advection by large-scale winds allows for disequilibrium in air-sea temperature and shifts responses of winds or stress as a function of the SST spatial scales and the large-scale wind direction and speed (e.g., Small et al. 2005a, 2008). Spectral transfer functions, or their

corresponding physical-space impulse response functions, capture these non-local relationships, and generalize the widely used coupling coefficients to include spatial lags. Estimates from satellite observed winds and SST of spectral transfer functions suggest scale-dependent, lagged dynamics as a function of the Rossby number determined by large-scale winds, the wavenumbers of ocean mesoscale SST and the Coriolis frequency f, or thermal or frictional adjustment rates γ or A/H^2 (Schneider 2020; Masunaga and Schneider 2021). For small Rossby numbers the pressure effect dominates, large Rossby numbers favor the vertical mixing effect, and order one Rossby numbers combine both with rotational effects, consistent with modeling studies of boundary layer responses to prototype SST fronts (Spall 2007; Kilpatrick et al. 2014, 2016) and ocean eddy fields (Foussard et al. 2019a) in the presence of large-scale winds.

The analytical model described above considers a dry MABL without incorporating MABL moisture or latent heat fluxes. The contribution of moisture to buoyancy fluxes, latent heating/cooling, and overall MABL structure has not been investigated in as much detail within the context of the mesoscale MABL response. However, it is anticipated to have a non-negligible impact on the MABL dynamical response to mesoscale SSTA (Skyllingstad and Edson 2009). For instance, during CLIMODE, the buoyancy heat flux was approximately 20% larger than the sensible heat flux due to moisture and the average magnitude of the latent heat flux was ~2.5 times greater than the sensible heat flux (Marshall et al. 2009). In the tropics, the ratio of latent to sensible heat flux is even larger (e.g., de Szoeke et al. 2015), so the moisture contribution is often an order of magnitude larger than the sensible heat contribution. The impact of moist convection during a cold air outbreak over the Gulf Stream was investigated with an LES (Skyllingstad and Edson 2009), showing that the latent and sensible heat fluxes are enhanced over a simulated SST front resulting in stronger turbulent mixing and precipitation compared to a constant SST simulation. The simulation across the SST front shows that relatively low humidity values near the surface are maintained by the continual expansion of the boundary layer in the entrainment layer, which mixes dry air from aloft into the MABL. This maintains the large air-sea specific humidity and temperature differences necessary for strong latent and sensible heat fluxes in the surface layer. Additional simulations and measurements are necessary to investigate the role of moisture in response to mesoscale SST. For example, the analytical model could provide insight by using the virtual temperature at both the sea surface and aloft.

d. Modulation of air-sea fluxes of tracers

Air-sea gas fluxes of tracers depend on the air-sea disequilibrium and processes driving exchange, such as winds and breaking waves. From the ocean perspective, the disequilibrium can be understood as the difference of the concentrations of a gas in the seawater, C, relative to the concentration the gas would have at equilibrium with the atmosphere, C_{eq}, which, in turn, is determined by the solubility of the gas in seawater. The air-sea flux Fthen is estimated as $F = k(C - C_{eq})$, where k is the gas transfer velocity (e.g., Woolf 1993; McGillis et al. 2001; Wanninkhof et al. 2009; Dong et al. 2021). Impacts of ocean mesoscale features on the net Fmay be introduced via k or C_{eq}, each of which varies nonlinearly with wind speed and depends on sea state. The mesoscale may also affect$C$by impacting biological sources and sinks of tracers (Section 4d). Indeed, studies find local modulations of air-sea CO_2 fluxes due to effects of mesoscale eddies on solubility, productivity, or winds (Jones et al. 2015; Song et al. 2015, 2016; Olivier et al. 2021). One such study in the Southwest Atlantic Ocean detected clear spatial covariations of CO_2 flux with the MABL stability over a warm-core eddy (Figure 2, Pezzi et al. 2021). Yet, on the basin-to-global scales, positive and negative mesoscale anomalies of CO_2 fluxes appear to largely cancel (Wanninkhof et al. 2011; Song et al. 2015). A clear separation and quantification of the individual and rectified effects of mesoscale phenomena on $k, C,$ and C_{eq} from observations and models remain challenging, given the difficulty to capture transient mesoscale variations in the ocean and atmosphere, including the concentration of tracers such as carbon.

3. Free-tropospheric, extratropical atmospheric circulation responses

This section investigates local and non-local atmospheric circulation responses to extratropical SSTA including WBC regions. We start with a summary of existing studies on the role of extratropical SSTA in quasi-equilibrium atmospheric circulation and storm tracks. We then discuss the ongoing debates about the observed near-surface wind convergence and precipitation in WBC regions diagnosed either as a response to SST variations or extratropical storms. Finally, we will consider whether these processes may be important to future climate, focusing on the difference between projections at high and low resolution in the oceans.

a. Time-mean general circulation responses

The question of how the extratropical atmosphere responds to variability in ocean fronts and/or extratropical SSTA has been addressed over many decades. Early studies considered the linear response (Hoskins and Karoly 1981; Frankignoul 1985), which predicted a shallow heating response characterized by a downstream trough with a baroclinic structure. This was argued against by Palmer and Sun (1985), who found a downstream ridge, with advection of temperature anomalies by mean flow acting against anomalous advection of mean temperature gradients. Later, Peng et al. (1997) showed that the transient eddy response was important in forming an equivalent barotropic high. More recent observational analyses find a weak low-pressure response east of warm SSTA near the Gulf Stream (Wills et al. 2016) and Kuroshio (Frankignoul et al. 2011; Wills and Thompson 2018). Deser et al. (2007) demonstrated that the initial linear, baroclinic response is quickly (within 2 weeks) replaced with the equilibrium barotropic response with a much broader spatial extent and magnitude (Ferreira and Frankignoul 2005, 2008; Seo et al. 2014). The adjustment time is shorter near WBC regions (Smirnov et al. 2015). This literature is well summarized in existing review papers (Kushnir et al. 2002; Small et al. 2008; Kwon et al. 2010; Czaja et al. 2019).

Recent studies also indicated a strong sensitivity on spatial resolution of the atmospheric dynamics governing the large-scale circulation response. Figure 3 from Smirnov et al. (2015) shows that a low-resolution (1°) model induces a weak response resulting from shallow anomalous heating balanced by equatorward cold air advection, consistent with the results from linear steady dynamics. This is in contrast to the higher resolution (1/4°) model showing that the anomalous diabatic heating is balanced by a deep vertical motion mediated by the transient eddies (Hand et al. 2014; Wills et al. 2016; Lee et al. 2018). The anomalous diabatic heating and the induced vertical motions maintain the climatological circulation pattern over the WBCs.

b. Synoptic storms and storm track responses

Midlatitude storm tracks can be largely defined in two ways (Chang et al. 2002; Hoskins and Hodges 2002): either using distributions of the tracks and intensity of synoptic cyclones (the Lagrangian view) or as regions of strong variability or co-variability of winds, geopotential height, temperature, and humidity (the Eulerian perspective). Storm tracks typically occur in the

30-50° latitude band coincident with the climatological SST fronts (Figure 4) and are associated with strong and frequent precipitation, particularly atmospheric fronts.

One possible mechanism of midlatitude oceanic influence on the storm track was suggested by Hoskins and Valdes (1990), who found that enhanced diabatic heating by surface fluxes over WBCs supports atmospheric baroclinicity, a vital element in setting the location of the storm track (Hawcroft et al. 2012; Kaspi and Schneider 2013). Nakamura and Shimpo (2004) and Nakamura et al. (2004) further argued that low-level air temperature gradients are directly influenced by SST gradients via cross-frontal gradients in sensible heat flux (See also Nakayama et al. 2021). The baroclinicity is measured as the maximum Eady growth rate (Charney 1947; Eady 1949; Lindzen and Farrell 1980), such that stronger low-tropospheric baroclinicity is associated with weaker static stability and a stronger meridional air temperature gradient. Both conditions can be observed over WBCs. Hence, the anchoring effect by cross-frontal differential heat supply from the ocean is consistent with the formation of a storm track (Nonaka et al. 2009; Hotta and Nakamura 2011), while diabatic heating over the warm portion of the WBC SST fronts to the warm and cold sectors of the cyclones supports the growth of transient baroclinic waves (e.g., Booth et al. 2012; Willison et al. 2013; Hirata and Nonaka 2021).

A common method to diagnose the SST forcing mechanism is to run a pair of AGCM simulations, one using observed SSTs (CONTROL), and another using a spatially-smoothed SST field with weaker gradients (SMOOTH), which also alters absolute SST. Alternatively, AGCMs are forced by shifting the latitude of the SST fronts or filtering mesoscale eddy SSTs. Such AGCM simulations indicate a strengthening of the storm track near the Kuroshio-Oyashio Extension (KOE) (Kuwano-Yoshida and Minobe 2017) and the Gulf Stream (O'Reilly et al. 2017) in CONTROL near the climatological maximum cyclogenesis (Figure 5). Altered storm activity over the WBC regions influences the intensity of the coastal storms, and thereby inland weather near the KOE (Nakamura et al. 2012; Hayasaki et al. 2013; Sugimoto et al. 2021), Gulf Stream (Infanti and Kirtman 2019; Hirata et al. 2019; Liu et al. 2020), and the Agulhas Current (Singleton and Reason 2006; Nkwinkwa Njouodo et al. 2018).

To better elucidate the forcing of near-surface weather by the oceans, other studies define the surface storm track as the variance of near-surface meridional winds (Booth et al. 2010, 2017; O'Neill et al. 2017; Small et al. 2019). The concept of the surface storm track stems from earlier scatterometer measurements illustrating a strong imprint of the free-tropospheric storm tracks in the surface wind fields over the warm WBCs (Sampe and Xie 2007; Bourassa et al. 2013). The reduced static stability and the induced vertical mixing within the MABL lead to the co-location of the surface storm track with the warm currents. The surface and free-tropospheric storm tracks are thus dynamically coupled via deep moist convection (Czaja and Blunt 2011).

Recent studies indicate that atmospheric mesoscale phenomena, such as atmospheric fronts, within the storm tracks strongly interact with the WBC fronts. Parfitt and Czaja (2016) used reanalysis data over the Gulf Stream, and Parfitt et al. (2016) used AGCM simulations over the KOE to argue that the cross-frontal sensible heat flux gradients across the SST fronts exert "thermal damping or strengthening" of atmospheric fronts depending on the space-time alignment between the SST gradients and atmospheric fronts. The dominant cross-frontal length-scale of the atmospheric fronts is comparable to that of the WBC SST fronts, enabling such direct scale-to-scale thermal exchanges between the SST fronts and atmospheric fronts. The most significant diabatic heating by surface fluxes is concentrated on the narrow space-time scales at which the cold sectors of the atmospheric front coincide with the warm sector of the SST fronts.

Other studies emphasize the limited role of SST fronts on extreme cyclones. Masunaga et al. (2020a,b) showed that storms and fronts of moderate-intensity are significant contributors to the time-mean convergence observed over the Gulf Stream and KOE. AGCM experiments by Tsopouridis et al. (2021) indicated that the direct impacts of sharp SST fronts on individual cyclones over the Gulf Stream and KOE are weak, although SST fronts induce significant indirect responses in large-scale environments in which storms form. Using an idealized analytic model, Reeder et al. (2021) showed that diabatic frontogenesis over the WBCs could lead to intensification of atmosphere fronts only when strong and rapidly propagating synoptic systems are not already in the environment.

Much uncertainty still remains in model simulations and observational analysis regarding the relative importance of SST gradients causing cross-atmospheric frontal sensible heat flux gradients vs. absolute SST affecting the large-scale condensational heating over warm currents. The nature of the forcing is key in assessing whether high-resolution climate models with sharp SST fronts are necessary. The SST contribution to the precipitation from the warm and cold sectors of extratropical cyclones differs in terms of magnitude and spatial distribution: larger and broader for the warm sectors and weaker and more "anchored" to the SST fronts for the cold sectors (Vannière et al. 2017). It is likely that the cold sector contribution has been dominating the sensitivity of relatively high-resolution (~50 km) AGCM simulations to SST smoothing. It remains an open question whether even higher resolution AGCMs might amplify a sensitivity from the dynamics of the warm sectors, including mesoscale instabilities developing on the warm conveyor belt (Czaja and Blunt 2011; Sheldon et al. 2017).

c. Near-surface wind convergence over the WBCs

A crucial part of the storm track response to SST is precipitation, which tends to cluster around the WBCs and is associated with high near-surface wind convergence (NSWC) and substantial vertical ascent. The climatological NSWC is observed to coincide with the ocean fronts and the Laplacians of SST and SLP, which indicates that the boundary layer process depicted by linear Ekman dynamics is germane to the observed NSWC and precipitation responses (Feliks et al. 2004; Minobe et al. 2008, 2010). However, the unambiguous attribution of NSWC to the steady Ekman-balanced mass adjustment mechanism is difficult due to the coexistence of extratropical storm tracks with the WBC currents, which also induce minima in the time-mean SLP Laplacian over the SST fronts (O'Neill et al. 2017).

O'Neill et al. (2015) show from QuikSCAT observations and a regional atmospheric model that linear boundary layer dynamics cannot explain the daily time-scale occurrence of NSWC since, on rain-free days, surface divergence dominates even though the SST Laplacian would indicate convergence. Using an extreme value filter, O'Neill et al. (2017) further show that NSWC and vertical motion over the Gulf Stream are highly skewed and consist of infrequent yet extreme surface convergence events and more frequent but weak, divergent events, such that the median surface flow field is weakly divergent or nearly non-convergent (Figure 6). Parfitt and Czaja

(2016) and Parfitt and Seo (2018) argue that much of the precipitation and NSWC are associated with atmospheric fronts given that only a weak near-surface divergence remains in longer time means when the contribution from atmospheric fronts is removed (Rousseau et al. 2021).

Current research emphasizes identifying how and why atmospheric fronts align with and linger over ocean fronts in all major WBCs and whether there is an additional underlying, steady, small-scale boundary layer effect. For example, Small et al. (unpublished manuscript) argue for a distinct temporal dependence of the NSWC over WBC SSTs, where atmospheric fronts govern its day-to-day variability, while the pressure adjustment and vertical mixing mechanisms provide lower frequency modulations. This is consistent with the results from Brachet et al. (2012), who separate the SLP Laplacian into sub-10 day and longer time-scales, showing the former being dominated by the synoptic disturbances and the latter the SST forcing.

d. Large-scale/downstream atmospheric circulation responses

Many AGCM studies demonstrate a non-local, downstream response in the storm track to WBC SST forcing. Wills et al. (2016) identified significant transient atmospheric circulation responses downstream that lag the SSTA in the Gulf Stream extension by several weeks. O'Reilly et al. (2016, 2017) found the northward shifted eddy-driven jet and the increased European blocking frequency in response to a strengthened storm track over the Gulf Stream. Along a similar line, Lee et al. (2018) suggested that SST biases near the Gulf Stream trigger extended biases in the simulation of deep convection and downstream circulation via Rossby wave response.

Similarly, O'Reilly and Czaja (2015) found that when the KOE front is in its stable regime featuring increased SST gradients, baroclinic eddies grow faster. The local shift in baroclinic wave activity leads to the early barotropitization of the baroclinic eddies downstream, resulting in weaker poleward eddy heat flux and increased occurrence of blocking in the eastern Pacific. An AGCM study by Kuwano-Yoshida and Minobe (2017) also suggested the enhanced storm track by the KOE SST fronts leads to a northward shifted storm track in the eastern Pacific. By considering only the transient SSTA due to KOE mesoscale eddies, Ma et al. (2015, 2017) showed that a northward shifted storm track led to reduced precipitation in parts of western North America during the eddy-active KOE years (Foussard al. 2019b; Liu et al. 2021; Siqueira

et al. 2021). In the Southern Ocean, Reason (2001) showed that amplified cyclone activity over the warm Agulhas Current yielded an enhanced storm track in the southeast Indian Ocean.

e. Climate change

Climate change simulations for the 21st Century have emphasized the critical role of ocean circulation leading to natural modes of variability such as ENSO and PDO (Seager et al. 2001), the predicted weakening of the Atlantic Meridional Overturning Circulation (AMOC; Weaver et al. 2012), and the delayed warming of the Southern Ocean (Marshall et al. 2014). These changes are relevant to a predicted intensification and poleward shift of the Kuroshio and Agulhas, weakening of the Gulf Stream, and changes in the frontal systems of the Antarctic Circumpolar Current (ACC) (e.g., Yang et al. 2016).

The IPCC report (IPCC, 2021) indicates that during the 21st Century, the North Pacific storm track will most likely shift poleward, the North Atlantic storm track is unlikely to have a simple poleward shift, and the Southern Hemisphere storm track will likely shift poleward. Understanding these regional differences in projected changes in midlatitude storm tracks and precipitation and their association with the predicted WBC changes have been the primary goals of high-resolution CGCM studies, especially those that contrast the CGCMs with eddy-rich ocean (typically 0.1º resolution) to those with eddy-parameterized ocean (0.5-1º). These studies with increased ocean model resolution to mitigate the known biases in representing the WBC dynamics and separation show distinct responses in SSTs and storm tracks in the WBC regions in response to anthropogenic climate change.

The Kuroshio front in the eddy-rich simulations shifted equatorward, contrary to projections by the IPCC-class CGCMs, which likely reflects the large natural variability in the North Pacific (Taguchi et al. 2007; Seager and Simpson 2016). In the North Atlantic, the Gulf Stream separation tends to be too far north in lower resolution models, but is improved in eddy-rich models. This makes it possible for the separation to move northwards as a response to AMOC weakening in eddy-rich models (Gervais et al. 2018; Moreno-Chamarro et al. 2021; Grist et al. 2021), leading to a significant projected ocean warming near the US eastern coastline (Figure 7; Karmalkar and Horton 2021). In the Southern Ocean, CMIP5-based climate change simulations

indicate delayed warming, which is often attributed to stratospheric ozone depletion (McLandress et al. 2011; Polvani et al. 2011). However, the recent satellite observations and eddy-rich CGCMs simulations indicate a ubiquitous cooling trend (1961-2005) poleward of the ACC due to resolved ocean eddies (Bilgen and Kirtman 2020). Analysis of eddy-rich ocean simulations also indicates warmer and stronger Southern Hemisphere WBCs, suggesting that resolved ocean eddies play a critical role in long-term SST changes.

The reorganization of the oceanic frontal zone and its associated eddy field modulates the low-level baroclinicity (Dacre and Gray 2013) and the strength and location of the diabatic heating source for the atmosphere. It is clear from this and other studies (Woollings et al. 2012; Winton et al. 2013; Keil et al. 2020) that such features would not occur in the absence of ocean circulation changes. However, the exact pattern of large-scale SST change is highly dependent on the ocean model and its resolution (Saba et al. 2016; Menary et al. 2018; Alexander et al. 2020), which also affects the projected WBC responses to climate change (Jackson et al. 2020). The climate projections with eddy-rich oceans have typically been performed with a small number of realizations and relatively short durations due to high computational cost (e.g., Haarsma et al. 2016). Currently, high-resolution coupled climate modeling projects are underway with much longer integration and multi-ensembles (e.g., Chang et al. 2020; Wengel et al. 2021). These efforts will enable a robust assessment of the forced responses in WBC and ocean circulation from natural variability in response to projected changes in the large-scale climate.

4. Feedback of atmospheric mesoscale responses onto the ocean

The new insights gained from these studies have led to improved process understanding and notable revisions of theories of ocean circulation. This section discusses current knowledge of ocean feedback mechanisms, feedback impacts on ocean biogeochemical cycles, and theories of ocean circulation and model parameterizations to account for eddy-atmosphere interaction.

a. Feedback to ocean circulation

For simplicity, we consider two categories of oceanic mesoscale effects on air-sea fluxes: SST impacts (thermal) described in Section 2b1, and surface current impacts (mechanical) in Section

2b2. The thermal feedback (TFB) results from kinematic and thermodynamic responses in the MABL to mesoscale SSTs, modifying the wind stress and heat fluxes. The current feedback (CFB) represents the processes by which the surface ocean current alters the wind stress, near-surface wind, and turbulent heat fluxes, and thereby ocean circulation.

1) Thermal feedback (TFB) effect

Observed near-surface wind stress responses to mesoscale processes by Chelton et al. (2004) were largely based on the TFB effect. Vecchi et al. (2004) and Chelton et al. (2007) hypothesized that the wind stress curl responses to SST fronts would constitute an important feedback mechanism driving ocean dynamics. Spall (2007) considered the impacts of SST-induced Ekman pumping on baroclinic instability in the modified linear theory by Eady (1949), showing that the SST-induced Ekman pumping adjusts the growth rate and wavelength of the most unstable waves, especially the low-latitude flows with strong stratification. Hogg et al. (2009) extended SST-induced Ekman pumping to an idealized double-gyre circulation in mid-latitudes, showing that it destabilizes the eastward jet with the enhanced cross-gyre potential vorticity fluxes, stabilizing the double gyre circulation by 30-40%.

Mesoscale SSTAs are damped by induced turbulent heat fluxes (THF), resulting in a negative SST-THF correlation at mesoscales (Figure 1b-c). Over the KOE, Ma et al. (2016) examined this mesoscale SSTA damping in the context of eddy potential energy (EPE) budget and the Lorentz energy cycle. Compared to the eddy-filtered coupled model simulation (using a 1000 km-by-1000 km boxcar filter), the eddy-unfiltered simulations showed a significant increase (>70%) diabatic EPE dissipation, leading to a decrease of EKE by 20-40%, most strongly at wavelengths shorter than 100 km. Other studies find that TFB has a weak impact on EKE (Seo et al. 2016; Seo 2017). The cause of this discrepancy is partially due to different filter cutoffs used to define the eddies. Renault et al. (unpublished manuscript) show that a large filter cutoff, as used in Ma et al. (2016), overestimates EKE damping and may also smooth large-scale meridional SST gradients, altering the large-scale wind curl and the mean oceanic circulation. Bishop et al. (2020) evaluated the EPE damping over the global oceans using eddy-resolving climate model simulations to find that the diabatic EPE damping was stronger over warm-core eddies.

2) Current feedback (CFB) effect

Surface currents, although weaker than surface winds, modify surface stress directly by altering wind speed (Bye 1986). In turn, by modulating the stress, the CFB exerts a "bottom-up" effect on the wind, where a positive current anomaly causes a positive wind anomaly via a negative stress anomaly (Renault et al. 2016a; 2019a). The CFB effect has initially focused on impact on wind stress. Using satellite and in situ data, Kelly et al. (2001) showed that CFB reduces the median wind stress from 20% to 50% near the equator, and Chelton et al. (2004) observed a clear imprint of the Gulf Stream flow on the surface stress and the curl.

Several studies have highlighted the role of CFB as a "top drag" (Dewar and Flierl 1987), acting on the oceanic circulation over a wide range of space-time scales. At the large-scale where the currents tend to flow downwind, CFB reduces the mean input of energy from the atmosphere to the ocean and therefore slows down the mean circulation (Pacanowski et al. 1997). By weakening net energy input to the ocean, CFB triggers a host of changes in eddy-mean flow interactions and the inverse cascade of energy, weakening baroclinic and barotropic instabilities and the mesoscale activity (Renault et al. 2017b, 2019a; Figure 8). When the wind and current are in the opposite sense, the CFB serves as a conduit of energy from the ocean to the atmosphere, which can be seen from satellite data as negative mean and eddy wind work (Figure 8a; Scott and Xu 2009; Renault et al. 2016a,b, 2017a). Numerous studies have demonstrated a strong EKE damping effect of ~30% (See references in Jullien et al. 2020; Figure 8b). CFB also induces additional Ekman pumping that weakens an eddy (Gaube et al. 2015) and influences the upper-ocean stratification (Seo et al. 2019; Song et al. 2020).

The role of CFB in ocean circulation modifies the classic concept of wind-driven currents. While the wind remains a large-scale energy source that initiates a turbulent cascade, its fine-scale interactions with currents also affect the entire oceanic spectrum. The route to dissipation in the ocean is still an open question. However, recent findings point to the role of mesoscale air-sea coupling via ocean currents that offers an unambiguous sink of energy to achieve proper equilibrium in ocean dynamics (Renault et al. 2016a; Fox-Kemper et al. 2019). Recent studies also have emphasized the CFB impact on near-surface winds (Renault et al. 2016a, 2017a, 2019a), which has led to an effort to accurately represent the CFB effect on air-sea momentum

exchanges in ocean-only models. Renault et al. (2020) tested new parameterizations that correct wind stress based on these coupling coefficients predicted from the wind magnitude, allowing replication of both wind and stress responses to CFB and the level of eddy energy from coupled simulations. As an indirect effect, CFB also exerts a strong control on WBC dynamics by weakening the inverse cascade of energy (Renault et al. 2019b).

There are a few remaining unknowns. First, little is known about CFB at the submesoscale. For the US West Coast, Renault et al. (2018) highlighted a submesoscale dual effect of CFB: it damps submesoscale eddies but also catalyzes submesoscale current generation. By affecting mixing, stratification, and eddy variability, CFB will modulate biogeochemical variability (McGillicuddy et al. 2007; Kwak et al. 2021). Since CFB and TFB coexist where mesoscale currents are strong (Song et al. 2006; Seo et al. 2007; Takatama and Schneider 2017; Renault et al. 2019b; Shi and Bourassa 2019), CFB likely influences large-scale boundary-layer moisture, clouds, precipitation, and atmospheric circulation via rectified effects. However, this downstream influence is only beginning to be explored (e.g., Seo et al. 2021). Finally, in the areas of strong tidal variability, tidal currents can exceed wind speed; whether the tidal current effect will be averaged out or whether it exerts a low-frequency rectified effect is an open question.

b. Impact of surface waves

While sea state is a salient aspect of air-sea fluxes (Fairall et al. 1996; Cavaleri et al. 2012; Edson et al. 2013), other aspects of wave interactions with (sub)mesoscale currents may be important for air-sea fluxes and regional circulation. It has long been known that sheared currents affect the propagation of surface wave rays (Villas Bôas and Young 2020). In the open ocean, the spatial gradients in mesoscale surface currents dominate the variability of significant wave height, leading to the refraction of waves near steep vorticity gradients (Ardhuin et al. 2017; Villas Bôas et al. 2020). Similarly, the underpinnings of the Craik-Leibovich theory of Langmuir turbulence specify that rectification of wave-vorticity interactions in the upper ocean leads to Stokes forces, which can cause substantial wave effects on currents (Leibovich et al. 1983; Lane et al. 2007). LES models that include vortex forces and regional models that include the wave refraction by currents (Romero et al. 2020) illustrate the frontal adjustment and frontogenesis triggered or enhanced by surface wave interactions (McWilliams and Fox-Kemper 2013; Suzuki et al. 2016;

Sullivan and McWilliams 2019). Examples are provided in Figure 9 (upper panel), where a submesoscale density front in the downwind and down-Stokes direction interacts with Langmuir turbulence. Strong overturning circulation (downwelling) sharpens the front and strengthens the along-front jet. Classic balances are altered by waves to yield the wavy Ekman balance (McWilliams et al. 2012), the wavy geostrophic balance (McWilliams and Fox-Kemper 2013, Figure 9, lower panel), and the baroclinic and symmetric instabilities affected by waves (Haney et al. 2015).

However, these studies of wave-induced mixing, frontogenesis, and instability do not yet fully take into account the impact of wave growth and breaking by the wind that is correlated with mesoscale SST gradients or ocean currents. Since both wave effects on currents and current effects on waves would strengthen as the fronts become smaller and more intense, emerging high-resolution fully-coupled model simulations that resolve fine-scale flow fields in the ocean are expected to represent this wave-current interaction better (Haney et al. 2015; Romero et al. 2020). The significance of these effects suggested by such models will motivate simultaneous observations of waves, currents, and air-sea fluxes to guide revised theories of wave-current interaction and validate high-resolution model simulations.

c. Ocean model physics

Traditionally, mesoscale and submesoscale eddy parameterizations have been deterministic and have focused only on effects on the mean and variance of tracers (Gent and McWilliams 1990; Fox-Kemper et al. 2011), while neglecting rectified effects on air-sea coupling. However, in simulations where some eddies are resolved, deterministic closures do not stimulate a resolved eddying response or backscatter (e.g., Bachman et al. 2020). In response, there is a growing desire to implement stochastic parameterizations of the eddy transport into non-eddy-resolving models, for example, via uncertainty in location (Memin 2014), transport (Drivas et al. 2020), closure (Nadiga 2008; Jansen and Held 2014; Zanna et al. 2017; Bachman et al. 2020), or equation of state (Brankart 2013). This can potentially include stochastic parameterizations of the air-sea coupling simultaneously. As stratification and rotation parameters vary globally, building scale awareness into parameterizations is also crucial (Hallberg 2013; Dong et al. 2020, 2021). Observed air-sea fluxes are highly variable, indicating a response to high spatio-temporal

variability (Yu 2019), scale dependence (Bishop et al. 2017, 2020), sea state dependence (Kudryavtsev et al. 2014), and thus offering the potential for stochastic implementation. While idealized studies have begun to develop a process-level understanding (Sullivan et al. 2020, 2021), at the time of this review, no realistic model implementation of stochastic air-sea fluxes seems to have been evaluated carefully.

d. Impacts on primary productivity

Mesoscale air-sea interaction can also influence biogeochemical environments and hence primary productivity (e.g., McGillicuddy 2016). The wind stress response to mesoscale SST and currents introduces perturbation Ekman upwelling and downwelling, leading to, for example, dramatic mid-ocean mesoscale plankton blooms in the nutrient-replete subtropics (McGillicuddy et al. 2007). Global satellite-based eddy-composite analyses demonstrate the widespread effect of mesoscale air-sea interaction on the ocean biogeochemical environment via eddy currents and SST (e.g., Gaube et al. 2015). Additionally, eddy-induced modifications of wind stress impact vertical mixing in the upper oceans. Eddy effects on mixed-layer depths are asymmetric between anticyclones and cyclones (e.g., Dufois et al. 2017; Hausmann et al. 2017). However, to what extent this asymmetry stems from the mesoscale modulations of surface wind stress has yet to be determined. Considering the prevalence and persistence of nonlinear mesoscale eddies in the global oceans (Chelton et al. 2011a,b), the relevance of mesoscale eddy impacts on primary productivity via eddy-wind interaction needs robust quantification.

5. State of observational capabilities

Observing mesoscale air-sea interaction processes is challenging since multiple oceanic and atmospheric parameters must be measured with high accuracy and spatio-temporal resolution. The past decade has seen the emergence of novel in situ and remote sensing platforms that will increasingly better capture mesoscale and smaller processes with high accuracy and resolution (e.g., Chapter 9 of Kessler et al. 2019). Here, we briefly discuss the existing and novel observational technologies that can provide multi-platform, coordinated measurements for air-sea interaction studies (e.g., Bony et al. 2017; Wang et al. 2018).

a. In situ observations

Oceanographic moorings can be equipped with meteorological instruments, including direct covariance flux system and bulk meteorological sensors to provide the directly measured and bulk-estimated air-sea fluxes, respectively. An example system is shown in Figure 10 from the second Salinity Processes in the Upper-ocean Regional Study (SPURS-2) experiment, which computed and telemetered in near-real-time the motion-corrected surface wind stress and sensible and latent heat fluxes from a surface mooring for the first time (Clayson et al. 2019). Recently, buoy arrays have been deployed as part of the Ocean Observatories Initiative (OOI, Trowbridge et al. 2019) and operated for years on both coasts. These data, along with the simultaneous measurements of surface meteorology and wave conditions, are crucial to reducing the uncertainty in air-sea flux estimates in modern bulk formulas (Cronin et al. 2019). Autonomous surface vehicles (ASVs) are piloted wave- or wind-propelled surface platforms that can be instrumented with ocean, atmospheric, and biogeochemical sensors. Widely-used ASVs include Saildrone (Meinig et al. 2019) and Wave Gliders (Thomson and Girton 2017), which have long endurance (~6 months) and can sample in remote locations and be piloted across fronts. The use of numerous instruments can mitigate issues with cross-frontal sampling and can thus capture mesoscale and smaller variations in air-sea interaction (Quinn et al. 2021; Stevens et al. 2021).

Drifting platforms can be instrumented with a variety of sensors that capture air-sea interaction. The Global Drifter Program, a global network of surface drifters that typically measure currents, SST, and barometric pressure, has contributed to the understanding of global mesoscale circulation (Laurindo et al. 2017; Centurioni et al. 2019). Drifting spar buoys (Graber et al. 2000; Edson et al. 2013) have been used to measure surface fluxes in situ for decades. In recent years, sophisticated low-profile Lagrangian platforms have been developed such as SWIFTs (Thomson 2012) to measure surface currents, waves, and near-surface ocean turbulence over a range of wave conditions. Benefits of drifters include relatively low cost and Lagrangian sampling. However, they tend to converge at fronts and therefore multiple drifters are necessary to characterize cross-frontal structure (D'Asaro et al. 2018).

Aircraft measurements have also been important for air-sea interaction studies. The mobility of the platform is advantageous because of its ability to obtain in situ measurements of the horizontal and vertical variability in and above the MABL in a short time. With carefully designed flight patterns, it can also derive mesoscale forcing to the boundary layer using the velocity field measured at flight level (Lenschow et al. 1999; Stevens et al. 2003). In the past 20 years, air-deployable sensor packages such as GPS dropsondes, AXBT, AXCTD, and instrumented floats have further expanded the sampling capability to depict the entire column of the atmosphere and the upper ocean, particularly when low-level flights are not feasible (Doyle et al. 2017). In recent years, airborne measurements have been extended down to 10 m above the sea surface using a controlled towed vehicle (Wang et al. 2018). This new capability is a significant addition to air-sea interaction studies, particularly on surface flux parameterization.

b. Remote sensing

Emerging remote sensing platforms, including satellite, ground-based, or airborne measurements, present promising means to estimate air-sea fluxes at ocean mesoscale and smaller. Scatterometer and microwave measurements provide global views of ocean vector winds and SST under all wind conditions at daily scales. However, under extreme conditions, large uncertainty exists due to inconsistent in situ reference wind speeds from dropsondes and moored buoys to calibrate satellite winds (e.g., Polverari et al. 2021). This also implies uncertainties in modeling ocean drag and air-sea interaction. The virtual constellation of scatterometers (Stoffelen et al. 2019) provides good temporal coverage of the extremes with now 7 scatterometers in space with revisits globally within 30 minutes or a few hours (Gade and Stoffelen 2019). Future satellite observations will need to resolve synoptic variability under strong wind and rain and increase the resolution of the vertical profiles within the MABL to better estimate the relationship between the surface flux and flux profiles.

For momentum fluxes, key variables are surface winds and currents. In coastal regions, high-frequency radar systems provide surface currents at O(1) km resolution (Paduan and Washburn 2013; Kirincich et al. 2019), which can be used to infer surface wave conditions and wind stress (e.g., Saviano et al. 2021). The airborne DopplerScatt system simultaneously captures surface wind stress, waves, and currents (Wineteer et al. 2020) and is central to the Sub-Mesoscale

Ocean Dynamics Experiment (S-MODE; Farrar et al. 2020). Similar measurement concepts have been proposed for new satellites (Villas Bôas et al. 2019), such as Harmony (López-Dekker et al. 2019), SeaStar (Gommenginger et al. 2019), and the Winds and Currents Mission (WaCM; Bourassa et al. 2016; Wineteer et al. 2020). Notably, the Harmony satellite mission relies on dual synthetic aperture radar (SAR) to measure surface roughness, enabling high-resolution detection of ocean fronts even in the presence of clouds. An increase in computing power and expansion of machine learning techniques (e.g., Wang et al. 2019) have the potential to improve the utility of SAR for air-sea interaction studies. Surface waves are also important in momentum flux estimates; new satellite missions such as CFOSAT (Chinese-French Oceanography Satellite) simultaneously measuring waves and winds (Ardhuin et al. 2019) are expected to improve the accuracy of the wind-speed and wave-based formulations in the modern flux bulk formula. Satellite surface measurements of stress-equivalent winds more closely respond to stress than wind (e.g., de Kloe et al. 2017). Given the persistent large-scale and mesoscale errors in NWP reanalyses (Belmonte and Stoffelen 2019; Trindade et al. (2020), these new satellite observations collocated with surface measurements of stress will be valuable for understanding stress-related air-sea coupling and improving ocean modeling and marine forecasting (Bourassa et al. 2019).

For turbulent heat fluxes, current satellite remote sensing systems rely on bulk parameterizations to represent net heat and gas fluxes (Bourassa et al. 2013; Cronin et al. 2019). Mesoscale air-sea interaction studies will benefit significantly from a satellite mission that measures co-located, small-scale state variables, including near-surface atmospheric temperature and humidity, SST, and wind speed to provide estimates of turbulent heat fluxes (e.g., Gentemann et al. 2020). This will also help validate the numerical models to lower the uncertainty in air-sea heat flux. As for the gas exchanges, new satellite missions, such as the Ka-band Doppler scatterometer that will simultaneously measure ocean vector winds, waves, and currents at 200 m spatial resolution, or the SWOT altimeter mission that will observe the dynamic topography at small mesoscales and can be combined with ocean color, will help elucidate the role of mesoscale air-sea interactions in biological and biogeochemical cycles in the coming years.

6. Summary and discussions

Since the first global-scale surveys of the mesoscale air-sea interactions by Chelton et al. (2004) and Xie (2004), our theoretical understanding and observational and modeling capabilities in the past two decades have advanced significantly, leading to a substantial body of literature related to mesoscale air-sea interaction. Our current scientific understanding indicates that mesoscale eddies actively perturb the MABL via surface flux anomalies leading to dynamic and thermodynamic adjustments (Section 2). The MABL response is communicated to the free troposphere, especially over WBCs, influencing downstream development of weather and short-term climate events (Section 3). The MABL response feeds back to the ocean circulation, influencing WBC dynamics, air-sea gas exchanges, and nutrient distribution (Section 4). This new knowledge has transformed our classical understanding of physical processes, leading to notable revisions of the theories of oceanic and atmospheric circulation (Section 4). Our observational capability is advancing rapidly to better characterize mesoscale air-sea interaction (Section 5). However, numerous challenges must be overcome to diagnose, observe, and simulate mesoscale air-sea interaction. Here is the notable list (non-exhaustive) of issues in theory, observations, and modeling that we think deserve some further comments.

a. Climate modeling and physical parameterizations

Significant progress has been made in understanding results and uncertainties in climate models of different complexity and resolutions mainly via coordinated modeling experiments with resolutions at or beyond the ocean mesoscale and common sets of diagnostics. The CMIP6 HighResMIP protocol was a step in this direction (Haarsma et al. 2016). Analyses from a subset of these models from the PRIMAVERA project (Bellucci et al. 2021) reveal model resolution sensitivity (especially in the oceans) of the simulated regimes of air-sea interaction and climate in the extratropics. For example, Moreton et al. (2021) show how modeled air-sea flux feedbacks can be damped depending on the relative ocean-atmosphere resolutions and coupling methods, emphasizing the need for understanding these numerical aspects and the bulk formula in flux calculations (See also Jullien et al. 2020). Further advances in model resolution, for example, DYAMOND (Stevens et al. 2019) and the planned HighResMIP2, together with programs such as OASIS (Observing Air-Sea Interaction Strategy, https://airseaobs.org) that aims to bring observations and models closer together, will build on these previous efforts and provide further

insights into the fidelity of modeled mesoscale air-sea interactions. Furthermore, in the ocean and coupled models where the ocean eddies are not fully or only partially resolved, their rectified effects on the air-sea heat and momentum fluxes are not currently parameterized. Various stochastic representations of eddy transports are being tested and implemented (Section 4c), which can potentially address this issue of low-frequency rectification effects by eddies on large-scale climate via air-sea interaction (e.g., Siqueira and Kirtman 2016).

b. Ocean biogeochemistry processes

Estimates of air-sea gas exchange of tracers do not fully consider effects arising from ocean mesoscale eddies and fronts. One issue is that the gas transfer velocity typically (i) does not consider wind variations introduced by mesoscale air-sea interactions, and (ii) is based on wind speed (e.g., Wanninkhof 1992), and hence only implicitly accounts for the sea state variations. Ocean mesoscale features influence the sea state and wind speeds, which are not always in equilibrium, so that local wind alone is insufficient to describe the wave impact on gas exchanges. Studies with parameterizations that consider bubble-mediated gas exchanges due to breaking waves (e.g., Frew et al. 2007; Deike and Melville 2018) reveal their significant contribution to regionally-integrated CO_2 flux especially under midlatitude storm tracks (e.g., Reichl and Deike 2020). To more accurately represent the sea state influence modulated by mesoscale processes in the transfer velocity-based flux parameterization (e.g., Fairall et al. 2011; Edson et al. 2011), it is imperative to increase direct measurements of CO_2 flux (e.g., McGillis et al. 2001) along with the coincident observations of wind, waves, solubility, and air-sea partial CO_2 pressure differences.

Further, physical mesoscale air-sea interaction is likely feed back to ocean primary productivity (see the reviews by Lévy 2008; McGillicuddy et al. 2016), thereby also affecting air-sea fluxes and tracer concentrations in the ocean, such as carbon. Mesoscale eddies are observed ubiquitously in the global oceans; however, their physical properties, and their relationships with biogeochemical variables, vary widely by region (e.g., Chelton et al. 2011; Gaube et al. 2013, 2014). Future work should aim to identify the specific aspects of this regional variability that are due to mesoscale air-sea interaction and subsequent impacts on upwelling and vertical mixing.

It remains unclear how important biogeochemical effects due to mesoscale air-sea interactions are for the larger-scale air-sea fluxes, biogeochemical mixed-layer properties, or ocean interior. Eddy-rich climate model simulations are one avenue to gain more insight into the relevance of the complex coupling of ocean mesoscale features, biogeochemistry, and the atmosphere. Few such simulations currently exist due to their computational expense (e.g., Harrison et al. 2018), but we expect this to change in the coming years. In addition, dedicated field experiments and process studies are critical to determining what aspects of mesoscale air-sea interactions need to be considered and represented in non-eddy-resolving models.

c. Submesoscale air-sea interaction

The ocean submesoscale processes with length-scales smaller than ~10 km are essential for the ocean energy cycle (Lorenz 1960), global heat balance (Su et al. 2018), and marine biogeochemistry and ecosystems (Omand et al. 2015; Lévy et al. 2018). While the dynamics of the submesoscale ocean instabilities are becoming better understood (e.g., Fox-Kemper et al. 2008; D'Asaro et al. 2011), their direct impact on the MABL and heat and carbon uptake by the oceans (e.g., Johnson et al. 2016; Bachman et al. 2017; du Plessis et al. 2019) are not as well understood. Thus far, only a few satellite-based studies provide direct observational evidence of relative wind stress response to submesoscale SST fronts (e.g., Beal et al. 1997; Xie et al. 2010; Gaube et al. 2019; Ayet et al. 2021), although in situ observational studies have long documented such interactions in localized regions (e.g., Sweet et al. 1981; Friehe et al. 1991; Mahrt et al. 2004). While results from high-resolution numerical simulations (e.g., LES) indicate SST-driven MABL dynamics (Skyllingstad et al. 2007; Lambaert et al. 2013; Wenegrat and Arthur 2018; Lac et al. 2018; Sullivan et al. 2020, 2021), they also recognize the importance of advection and convective organization to characterize nonlinear MABL dynamics at the submesoscale. As for the oceanic impact, the ocean current feedback dominates the wind stress response at the submesoscale, which influences the submesoscale flow fields and ocean kinetic energy (Renault et al. 2018). Spatial variability in sea state and surface roughness are enhanced at the submesoscale, and hence wave-current interactions (e.g., Villas Bôas and Pizzo 2021) and wave-wind interactions (e.g., Deskos et al. 2021) are expected to be critical in determining wind stress, heat flux, and MABL variations (Ayet et al. 2021). Emerging in situ and satellite observations for near-surface processes (Section 5) should be combined with dedicated atmospheric and

oceanic LES and high-resolution modeling studies for boundary layer turbulence to improve the physical understanding of air-sea interactions at the submesoscale.

d. Climatological near-surface wind convergence

There are some remaining questions regarding the essential role of WBC SST forcing on the time-mean atmospheric state. The ongoing debates about the origin of the near-surface wind convergence (NSWC) and the maximum precipitation over WBCs are particularly relevant as they entail important implications pertinent to various aspects of the topics discussed in this article. That is, to assess whether or not the steady linear boundary layer dynamics accounts for the time-mean NSWC and vertical motion requires a detailed understanding of the modulation of boundary layer ageostrophic circulation by SST (Section 2). On the other hand, the demonstrated impacts of storms and atmospheric fronts on the NSWC require a careful examination of extratropical cyclogenesis modulated by the diabatic forcing over the ocean fronts (Section 3). Overall, any approach to quantifying the nature of the relationships between time-mean convergence and SST will need to robustly separate the small magnitude convergence predicted by linear boundary layer theory from the anomalous convergence induced by storm systems that are several orders of magnitude greater.

e. Diagnostics for air-sea interactions

The debate about the role of SST fronts in the NSWC arises partly due to the lack of a robust process-based diagnostics and analytic framework to interpret the observed convergence patterns. The existing analytical model of Schneider and Qiu (2015) discussed in Section 2c offers a complete account of the role of boundary layer dynamics over the SST fronts, which provides the two limiting cases of wind response to SST dependent on background wind speed. The model also suggests an extension of the diagnostic framework from the widely used coupling coefficients to lagged regression, impulse response, or corresponding spectral transfer functions. Yet, the model assumes a quasi-steady state and does not account for the processes associated with the storm tracks and their synoptic-scale influence on NSWC. A critical path forward is to incorporate the time-dependent or stochastic processes related to storms along SST frontal zones and the local SST-induced boundary layer response in a single analytical framework. Given the coexistence of the SST and current feedback effects along the frontal

zones, such diagnostic frameworks will also have to consider the mechanical coupling effects simultaneously along with the thermal effects (e.g., Takatama and Schneider 2017).

f. Downstream atmospheric circulation responses

Despite numerous studies suggesting WBC impacts on downstream atmospheric circulation, the nature of the far-field circulation response to WBC SST forcing and its statistical significance remains uncertain (Kushnir et al. 2002; Kwon et al. 2010; Czaja et al. 2019). Some studies argue that the sharpness of WBC fronts shifts the storm track and jet stream, influencing the blocking frequency in Europe and Northeastern Pacific (e.g., Kuwano-Yoshida and Minobe 2017; O'Reilly et al. 2015, 2016, 2017; Piazza et al. 2016). Other studies find that meridional shifts of WBC fronts alter the basin-scale transient eddy heat flux (e.g., Frankignoul et al. 2011; Kwon and Joyce 2013; Seo et al. 2017). Warm-core eddies near the KOE act as significant oceanic sources of moisture and heat for large-scale circulation, altering downstream precipitation patterns (Ma et al. 2015, 2016; Liu et al. 2021). Deriving a robust conclusion on downstream influences from these studies remains difficult since they adopt different methods to define WBC SST impacts, leading to distinct amplitudes/patterns of SST perturbations, and thus different atmospheric responses (this uncertainty is in addition to differences in model climatologies). Large-scale circulation will likely respond differently to different aspects of WBC SST variability. To date, the relative impacts of sharpness of SST gradient, its meridional shift, and activity of warm or cold-core eddies remain unquantified. The coordinated multi-model, common-forcing simulation and diagnostic framework, akin to PRIMAVERA/HighResMIP (Section 6a), will be extremely valuable in this regard, particularly with large ensemble sizes and long integrations to produce statistical robustness.

g. Final remarks

Prospects for significant advances in mesoscale air-sea interaction in the coming years are extremely bright. Currently, strong community efforts and enthusiasm exist for building sustained observational networks to characterize detailed physical and biogeochemical processes across the air-sea coupled boundary layers (e.g., OceanObs'19 White Papers; OASIS). New satellite missions with advanced instrument technology and retrieval algorithms continue to be developed to improve our capability to monitor state variables pertinent to air-sea interactions at

fine scales and high accuracy. These new observations lead to updated physical parameterizations that are increasingly more scale-aware and potentially built with stochastic schemes that account for rectified effects of eddy transports on air-sea flux and large-scales. More field experiments are being designed with close integration with process-oriented and data assimilative modeling to help not only design the sampling plans but also improve the parameterizations and skills in prediction models (e.g., Cronin et al. 2009; Cravatte et al. 2016; Kessler et al. 2019; Sprintall et al. 2020; Shroyer et al. 2021; Shinoda et al. 2021). The climate modeling community is developing and refining high-resolution Earth system model simulations with advanced physical parametrizations. International partnership and coordination are becoming ever more solid, enabling the design of multi-model, multi-ensemble, high-resolution coupled modeling protocols and diagnostic frameworks. The identified common biases in mesoscale air-sea interaction in such climate models, in turn, guide the sampling strategy of observing systems and process studies. Ensemble data assimilation systems are rapidly advancing, yielding more accurate observationally constrained ocean, atmosphere, and biogeochemical state estimates critical for sub-seasonal to decadal predictions (e.g., Penny and Hamill 2017; Verdy and Mazloff 2017). Overall, the successful coordination across observations, modeling, and theories has been critical, and these coordinated efforts will and should continue to enhance Earth system prediction skills from weather forecasts to climate projection scales.

Acknowledgments

The authors of the paper are the scientists participating in the US CLIVAR Working Group on *Mesoscale and frontal-scale ocean-atmosphere interactions and influence on large-scale climate*. The authors thank Mike Patterson and Jennie Zhu at US CLIVAR for sponsoring the Working Group activities. We acknowledge Susan Sholi (WHOI) for her assistance in editing the final manuscript.

References

Alexander, M. A., and J. D. Scott, 1997: Surface flux variability over the North Pacific and North Atlantic Oceans. *J. Climate*, **10**, 2963-2978.

Alexander, M. A., S. Shin, J. D. Scott, E. Curchitser, and C. Stock, 2020: The Response of the Northwest Atlantic Ocean to Climate Change. *J. Climate*, **33**, 405-428.

Ardhuin, F., S. T. Gille, D. Menemenlis, C. B. Rocha, N. Rascle, B. Chapron, J. Gula, and J. Molemaker, 2017: Small-scale open ocean currents have large effects on wind wave heights. *J. Geophys. Res. Oceans*, **122**, 4500–4517.

Ardhuin, F., and Coauthors, 2019: Observing Sea States. *Front. Mar. Sci*. **6**, 124.

Ayet, A., N. Rascle, B. Chapron, F. Couvreux, and L. Terray, 2021: Uncovering air-sea interaction in oceanic submesoscale frontal regions using high-resolution satellite observations. *US CLIVAR Variations*, **19**, 10-17.

Bachman, S. D., J. R. Taylor, K. A. Adams, and P. J. Hosegood, 2017: Mesoscale and Submesoscale Effects on Mixed Layer Depth in the Southern Ocean. *J. Phys. Oceanogr*, **47**, 2173-2188.

Bachman, S. D., B. Fox-Kemper, and F. O. Bryan, 2020: A diagnosis of anisotropic eddy diffusion from a high-resolution global ocean model. *J. Adv. Model. Earth Syst.*, **12**, e2019MS001904.

Battisti, D., E. Sarachik, and A. Hirst, 1999: A consistent model for the large-scale steady surface atmospheric circulation in the tropics. *J. Climate*, **12**, 2956–2964.

Beal, R. C., V. N. Kudryavtsev, D. R. Thompson, S. A. Grodsky, D. G. Tilley, V. A. Dulov, and H. C. Graber, 1997: The influence of the marine atmospheric boundary layer on ERS 1 synthetic aperture radar imagery of the Gulf Stream. *J. Geophys. Res.*, **102**, 5799– 5814.

Bellucci, A., Athanasiadis, P., Scoccimarro, E., Ruggieri, P., Gualdi, S., Fedele, R., Haarsma, R. J., Garcia-Serrano, J., Castrillo, M., Putrasahan, D., Sanchez-Gomez E., Moine, M.-P., Roberts, C. D.,Roberts, M. J., Seddon, J., and Vidale, P. L., 2021: Air-Sea interaction over the Gulf Stream in an ensemble of HighResMIP present climate simulations. *Clim Dyn*., **56**, 2093–2111.

Belmonte Rivas, M., and A. Stoffelen, 2019: Characterizing ERA-interim and ERA5 surface wind biases using ASCAT. *Ocean Sci. Discuss.*, **15**, 831–852.

Bilgen, S. I., and B. P. Kirtman, 2020: Impact of ocean model resolution on understanding the delayed warming of the Southern Ocean. *Environ. Res. Lett.*, **15**, 114012.

Bishop, S. P., R. J. Small, F. O. Bryan, and R. A. Tomas, 2017: Scale dependence of mid-latitude air-sea interaction. *J. Climate,* **30**, 8207–8221.

Bishop, S. P., R. J. Small, and F. O. Bryan, 2020: The global sink of available potential energy by mesoscale air-sea interaction. *J. Adv. Model. Earth Syst.*, **12**, e2020MS002118.

Bladé, I., 1997: The Influence of Midlatitude Ocean-Atmosphere Coupling on the Low-Frequency Variability of a GCM. Part I: No Tropical SST Forcing. *J. Climate*, **10**, 2087-2106.

Bony, S., Stevens, B., Ament, F. et al., 2017: EUREC4A: A Field Campaign to Elucidate the Couplings Between Clouds, Convection and Circulation. *Surv. Geophys.*, **38**, 1529–1568.

Bourassa, M. A., and Coauthors, 2013: High-latitude ocean and sea ice surface fluxes: requirements and challenges for climate research. *Bull. Amer. Meteo. Soc.*, **94**, 403–423.

Bourassa, M. A., E. Rodríguez, and D. B. Chelton, 2016: Winds and Currents Mission: Ability to observe mesoscale AIR/SEA coupling. *Geosci. and Remote Sens. Symposium (IGARSS)*, doi: 10.1109/IGARSS.2016.7730928.

Bourassa, M. A., and Coauthors 2019: Remotely Sensed Winds and Wind Stresses for Marine Forecasting and Ocean Modeling. *Front. Mar. Sci.*, **6**, 443.

Booth, J. F., L. Thompson, J. Patoux, K. A. Kelly, and S. Dickinson, 2010: The signature of midlatitude tropospheric storm tracks in the surface winds. *J. Climate*, **23**, 1160–1174.

Booth, J. F., L. Thompson, J. Patoux, and K. A. Kelly, 2012: Sensitivity of midlatitude storm intensification to perturbations in the sea surface temperature near the Gulf Stream. *Mon. Wea. Rev.*, **140**, 1241–1256.

Booth, J. F., Y. O. Kwon, S. Ko, R. J. Small, and R. Msadek, 2017: Spatial patterns and intensity of the surface storm tracks in CMIP5 models. *J. Climate*, **30**, 4965–4981.

Brachet, S., F. Codron, Y. Feliks, M. Ghil, H. Le Treut, and E. Simonnet, 2012: Atmospheric Circulations Induced by a Midlatitude SST Front: A GCM Study. *J. Climate*, **25**, 1847–1853.

Brankart, J.-M., 2013: Impact of uncertainties in the horizontal density gradient upon low resolution global ocean modelling. *Ocean Modell.*, **66**, 64-76.

Bryan, F. O., R. Tomas, J. M. Dennis, D. B. Chelton, N. G. Loeb, and J. L. McClean, 2010: Frontal Scale Air-Sea Interaction in High-Resolution Coupled Climate Models. *J. Climate*, **23**, 6277-6291.

Bye, J. A. T., 1986: Momentum exchange at the sea surface by wind stress and understress. *Quart. J. Roy. Met. Soc.*, **112**, 501–510.

Cavaleri, L., B. Fox-Kemper, and M. Hemer, 2012: Wind waves in the coupled climate system. *Bull. Amer. Meteorol. Soc.*, **93**, 1651–1661.

Centurioni, L. R. and Coauthors, 2019: Global in situ Observations of Essential Climate and Ocean Variables at the Air-Sea Interface. *Front. Mar. Sci*., **6**, 419.

Chang, E. K. M., S. Lee, and K. L. Swanson, 2002. Storm Track Dynamics. *J. Climate,* **15**, 2163-2183.

Chang, P., and Coauthors, 2020: An unprecedented set of high-resolution Earth system simulations for understanding multiscale interactions in climate variability and change. *J. Adv. Model. Earth Sys*. **12**, e2020MS002298.

Charney, J. G., 1947: The dynamics of long waves in a baroclinic westerly current. *J. Meteor.*, **4**, 135–162.

Chelton, D. B., and Coauthors, 2001: Observations of coupling between surface wind stress and sea surface temperature in the eastern tropical Pacific. *J. Climate,* **14**, 1479–1498.

Chelton, D. B., M. G. Schlax, M. H. Freilich, and R. F. Milliff, 2004: Satellite measurements reveal persistent small-scale features in ocean winds. *Science*, **303**, 978–983.

Chelton, D. B., 2005: The Impact of SST Specification on ECMWF Surface Wind Stress Fields in the Eastern Tropical Pacific. *J. Climate*, **18**, 530-550.

Chelton, D. B., M. G. Schlax and R. M. Samelson, 2007: Summertime Coupling between Sea Surface Temperature and Wind Stress in the California Current System. *J. Phys. Oceanogr*., **37**, 495-517.

Chelton, D. B., and S.-P. Xie, 2010: Coupled ocean-atmosphere interaction at oceanic mesoscales. *Oceanogr*., **23**, 52-69.

Chelton, D. B., P. Gaube, M. G. Schlax, J. J. Early, and R. M. Samelson, 2011a: The Influence of Nonlinear Mesoscale Eddies on Near-Surface Oceanic Chlorophyll. *Science*, **334**, 328–332.

Chelton, D. B., M. G. Schlax, and R. M. Samelson, 2011b: Global observations of nonlinear mesoscale eddies. *Prog. Oceanogr*., **91**, 167-216.

Clayson, C. A., J. B. Edson, A. Paget, R. Graham, and B. Greenwood, 2019: The effects of rainfall on the atmosphere and the ocean during SPURS-2. *Oceanogr.*, **32**, 86–97.

Cravatte, S., W. S. Kessler, N. Smith, S. E. Wijffels, and Contributing Authors, 2016: First Report of TPOS 2020. GOOS-215, 200 pp. [Available online at http://tpos2020.org/first-report/.]

Cronin, M. F., S.-P. Xie, and H. Hashizume, 2003: Barometric pressure variations associated with eastern Pacific tropical instability waves. *J. Climate*, **16**, 3050- 3057.

Cronin, M. F., S. Legg, and P. Zuidema, 2009: Best practices for process studies. *Bull. Amer. Meteor. Soc.*, **90**, 917–918.

Cronin, M. F., and Coauthors, 2019: Air-Sea Fluxes with a Focus on Heat and Momentum. *Front. Mar. Sci.*, **6**, 430.

Czaja, A., and N. Blunt, 2011: A new mechanism for ocean-atmosphere coupling in midlatitudes. *Quart. J. Roy. Met. Soc.*, **137**, 1095–1101.

Czaja, A., C. Frankignoul, S. Minobe, and B. Vannière, 2019: Simulating the Midlatitude Atmospheric Circulation: What Might We Gain From High-Resolution Modeling of Air-Sea Interactions? *Curr. Clim. Change Rep.*, **5**, 390–406.

Dacre, H. F., and S. L. Gray, 2013: Quantifying the climatological relationship between extratropical cyclone intensity and atmospheric precursors. *Geophys. Res. Lett.*, **40**, 2322– 2327.

D'Asaro, E., C. Lee, L. Rainville, R. Harcourt, and L. Thomas, 2011: Enhanced Turbulence and Energy Dissipation at Ocean Fronts. *Science*, **332**, 318-322.

D'Asaro, E., and Coauthors, 2018: Ocean convergence and dispersion of flotsam. *Proc. Natl. Acad. Sci.*, **115**, 1162–1167.

Davis, C. A., and K. A. Emanuel, 1988: Observational Evidence for the Influence of Surface Heat Fluxes on Rapid Maritime Cyclogenesis. *Mon. Wea. Rev*., **116**, 2649-2659.

de Boyer Montégut, C., G. Madec, A. S. Fischer, A. Lazar, and D. Iudicone, 2004: Mixed layer depth over the global ocean: An examination of profile data and a profile-based climatology. *J. Geophys. Res*., **109**, C12003.

de Kloe, J., A. Stoffelen, and A. Verhoef, 2017: Improved use of scatterometer measurements by using stress-equivalent reference winds. *IEEE J. Sel. Top. Appl. Earth Observ. Remote Sens*., **10**, 2340–2347.

de Szoeke, S. P., and C. S. Bretherton, 2004: Quasi-Lagrangian large eddy simulations of cross-equatorial flow in the east Pacific atmospheric boundary layer. *J. Atmos. Sci*., **61**, 1837-1858.

de Szoeke, S. P., and E. D. Maloney, 2020: Atmospheric Mixed Layer Convergence from Observed MJO Sea Surface Temperature Anomalies. *J. Climate*, **33**, 547-558.

de Szoeke, S. P., J. B. Edson, J. R. Marion, C. W. Fairall, and L. Bariteau, 2015: The MJO and Air–Sea Interaction in TOGA COARE and DYNAMO. *J. Climate*, 28, 597–622.

Deike, L., and W. K. Melville, 2018: Gas transfer by breaking waves. *Geophys. Res. Lett.*, **45**, 10,482–10,492.

Deser, C., R. A. Tomas, and S. Peng, 2007: The Transient Atmospheric Circulation Response to North Atlantic SST and Sea Ice Anomalies. *J. Climate*, **20**, 4751-4767.

Deskos, G., J. C. Y. Lee, C. Draxl, and M. A. Sprague, 2021: Review of wind-wave coupling models for large-eddy simulation of the marine atmospheric boundary layer. *J. Atmos. Sci*., **78**, 3025-3045

Dewar, W., and G. Flierl, 1987: Some effects of the wind on rings. *J. Phys. Oceanogr*., **17**, 1653–1667.

Dong, J., B. Fox-Kemper, H. Zhang, and C. Dong, 2020: The scale of submesoscale baroclinic instability globally. *J. Phys. Oceanogr.*, **50**, 2649–2667.

Dong, J., B. Fox-Kemper, H. Zhang, and C. Dong, 2021: The Scale and Activity of Symmetric Instability Estimated from a Global Submesoscale-Permitting Ocean Model. *J. Phys. Oceanogr*., **51**, 1655-1670.

Doyle, J. D., and Coauthors, 2017: A view of tropical cyclones from above: The Tropical Cyclone Intensity Experiment. *Bull. Amer. Meteor. Soc*., **98**, 2113–2134.

Drivas, T. D., D. D. Holm, and J. M. Leahy, 2020: Lagrangian Averaged Stochastic Advection by Lie Transport for Fluids. *J. Stat. Phys.*, **179**, 1304–1342.

du Plessis, M., S. Swart, I. J. Ansorge, A. Mahadevan, and A. F. Thompson, 2019: Southern Ocean Seasonal Restratification Delayed by Submesoscale Wind–Front Interactions. *J. Phys. Oceanog*r., **49**, 1035-1053.

Dufois, F., N. J. Hardman-Mountford, M. Fernandes, B. Wojtasiewicz, D. Shenoy, D. Slawinski, M. Gauns, J. Greenwood, and R. Toresen, 2017: Observational insights into chlorophyll distributions of subtropical South Indian Ocean eddies. *Geophys. Res. Lett.*, **44**, 3255–3264.

Eady, E., 1949: Long waves and cyclone waves. *Tellus*, **1**, 33–52.

Edson, J. B., and C. W. Fairall, 1998: Similarity relationships in the marine atmospheric surface layer for terms in the TKE and scalar variance budgets. *J. Atmos. Sci.*, **55**, 2311– 2328.

Edson, J. B., C. W. Fairall, L. Bariteau, C. J. Zappa, A. Cifuentes-Lorenzen, W. M. McGillis, S. Pezoa, J. E. Hare, and D. Helmig, 2011: Direct-covariance measurement of CO2 gas transfer velocity during the 2008 Southern Ocean Gas Exchange Experiment. *J. Geophys. Res*., **116**, C00F10.

Edson, J. B., V. Jampana, R. Weller, S. Bigorre, A. Plueddemann, C. Fairall, S. Miller, L. Mahrt, D. Vickers, and H. Hersbach, 2013: On the exchange of momentum over the open ocean. *J. Phys. Oceanogr*., **43**, 1589–1610.

Fairall C. W., E. F. Bradley, D. P. Rogers, J. D. Edson, and G. S. Young, 1996: Bulk parameterization of air-sea fluxes for Tropical Ocean Global Atmosphere Coupled-Ocean Atmosphere Response Experiment. *J. Geophys. Res.*, **15**, 3747-3764.

Fairall, C.W., E.F. Bradley, J.E. Hare, A.A. Grachev, and J.B. Edson, 2003: Bulk parameterization of air-sea fluxes: Updates and verification for the COARE algorithm. *J. Climate*, **16**, 571-591.

Fairall, C. W., M. Yang, L. Bariteau, J. B. Edson, D. Helmig, W. McGillis, S. Pezoa, J. E. Hare, B. Huebert, and B. Blomquist, 2011: Implementation of the COARE algorithm with O3, CO2 and DMS. *J. Geophys. Res.*, **116**, C00F09.

Farrar, J. T., and Coauthors, 2020: S-MODE: The Sub-Mesoscale Ocean Dynamics Experiment. *IGARSS 2020-2020 IEEE International Geoscience and Remote Sensing Symposium*. 3533-3536. 10.1109/IGARSS39084.2020.9323112.

Feliks, Y., M. Ghil, and E. Simonnet, 2004: Low-frequency variability in the midlatitude atmosphere induced by an oceanic thermal front. *J. Atmos. Sci*., **61**, 961–981.

Ferreira, D., and C. Frankignoul, 2005: The transient atmospheric response to midlatitude SST anomalies. *J. Climate*, **18**, 1049-1067.

Ferreira, D., and C. Frankignoul, 2008: Transient atmospheric response to interactive SST anomalies. *J. Climate*, **21**, 584-592.

Fox-Kemper, B., R. Ferrari, and R. Hallberg, 2008: Parameterization of mixed layer eddies. I: Theory and diagnosis. *J. Phys. Oceanogr.*, **38**, 1145-1165.

Fox-Kemper, B., G. Danabasoglu, R. Ferrari, S. M. Griffies, R. W. Hallberg, M. M. Holland, M. E. Maltrud, S. Peacock, and B. L. Samuels, 2011: Parameterization of mixed layer eddies. III: Implementation and impact in global ocean climate simulations. *Ocean Modell.*, **39**, 61-78.

Fox-Kemper, B., S. Marsland, E. Chassignet, E. Curchitser, S. Griffies, I. Montes, H. Seo, A. M. Treguier, and W. Weijer, 2019: Sources and sinks of ocean mesoscale eddy energy. 5, page 21. A Joint US CLIVAR and CLIVAR Workshop Report. Available from http://dx.doi.org/10.5065/CH5R-5034.

Foussard, A., G. Lapeyre, and R. Plougonven, 2019a: Response of surface wind divergence to mesoscale SST anomalies under different wind conditions. *J. Atmos. Sci.*, **76**, 2065-2082.

Foussard, A., G. Lapeyre, and R. Plougonven, 2019b: Storm Track Response to Oceanic Eddies in Idealized Atmospheric Simulations. *J. Climate*, **32**, 445-463.

Frankignoul, C., 1985: Sea surface temperature anomalies, planetary waves, and air-sea feedback in midlatitudes. *Rev. Geophys.*, **23**, 357–390.

Frankignoul, C., and K. Hasselmann, 1977; Stochastic climate models, Part II Application to sea-surface temperature anomalies and thermocline variability. *Tellus*, **29**, 289-305.

Frankignoul, C., N. Sennechael, Y.-O. Kwon, and M. A. Alexander, 2011: Influence of the meridional shifts of the Kuroshio and the Oyashio Extensions on the atmospheric circulation. *J. Climate*, **24**, 762–777.

Frenger, I., N. Gruber, R. Knutti, and M. Münnich, 2013: Imprint of Southern Ocean eddies on winds, clouds and rainfall. *Nature Geosci*., **6**, 608–612.

Frew, N. M., D. M. Glover, E. J. Bock, and S. J. McCue, 2007: A new approach to estimation of global air-sea gas transfer velocity fields using dual-frequency altimeter backscatter. *J. Geophys. Res*., **112**, C11003.

Friehe, C. A., W. J. Shaw, D. P. Rogers, K. L. Davidson, W. G. Large, S. A. Stage, G. H. Crescenti, S. J. S. Khalsa, G. K. Greenhut, and F. Li, 1991: Air-sea fluxes and surface layer turbulence around a sea surface temperature front, *J. Geophys. Res*., **96**, 8593–8609.

Gade, M., and A. Stoffelen, 2019: An Introduction to Microwave Remote Sensing of the Asian Seas. In: Barale V., Gade M. (eds) Remote Sensing of the Asian Seas. Springer, Cham. https://doi.org/10.1007/978-3-319-94067-0_4.

Gaube, P., D. B. Chelton, P. G. Strutton, and M. J. Behrenfeld, 2013: Satellite observations of chlorophyll, phytoplankton biomass, and Ekman pumping in nonlinear mesoscale eddies. *J. Geophys. Res. Oceans*, **118**, 6349–6370.

Gaube, P., D. J. McGillicuddy, D. B. Chelton, M. J. Behrenfeld, and P. G. Strutton, 2014: Regional variations in the influence of mesoscale eddies on near-surface chlorophyll. *J. Geophys. Res. Oceans*, **119**, 8195-8220.

Gaube, P. D. B. Chelton, R. M. Samelson, M. G. Schlax, and L. W. O'Neill, 2015: Satellite Observations of Mesoscale Eddy-Induced Ekman Pumping. *J. Phys. Oceanogr.*, **45**, 104–132.

Gaube, P., C. C. Chickadel, R. Branch, and A. Jessup, 2019: Satellite observations of SST-induced wind speed perturbation at the oceanic submesoscale. *Geophys. Res. Lett.*, **46**, 2690–2695.

Gent, P. R., and J. C. McWilliams, 1990: Isopycnal Mixing in Ocean Circulation Models. *J. Phys. Oceanogr*, **20**, 150-155.

Gentemann, C., C. A. Clayson, S. Brown, T. Lee, R. Parfitt, J. T. Farrar, M. Bourassa, P. J. Minnett, H. Seo, S. T. Gille, and V. Zlotnicki, 2020: FluxSat: Measuring the ocean-atmosphere turbulent exchange of heat and moisture from space. *Remote Sens.*, **12**, 1796.

Gervais, M., J. Shaman, and Y. Kushnir, 2018: Mechanisms Governing the Development of the North Atlantic Warming Hole in the CESM-LE Future Climate Simulations. *J. Climate*, **31**, 5927-5946.

Graber, H. C., E. A. Terray, M. A. Donelan, W. M. Drennan, J. C. Van Leer, and D. B. Peters, 2000: ASIS—A New Air–Sea Interaction Spar Buoy: Design and Performance at Sea. *J. Atmos. Ocean Tech.*, **17**, 708-720.

Gommenginger, C., and Coauthors, 2019: SEASTAR: A Mission to Study Ocean Submesoscale Dynamics and Small-Scale Atmosphere-Ocean Processes in Coastal, Shelf and Polar Seas. *Front. Mar. Sci.*, **6**, 457.

Grist, J. P., S. A. Josey, B. Sinha, J. L. Catto, M. J. Roberts, and A. C. Coward, 2021: Future evolution of an eddy rich ocean associated with enhanced east Atlantic storminess in a coupled model projection. *Geophys. Res. Lett.*, **48**, e2021GL092719.

Haarsma, R. J., M. Roberts and Coauthors, 2016: High Resolution Model Intercomparison Project (HighResMIP). *Geosci Model Dev*., **9**, 4185–4208.

Hallberg, R., 2013: Using a resolution function to regulate parameterizations of oceanic mesoscale eddy effects. *Ocean Modell*., **72**, 92-103.

Hand, R., and Coauthors, 2014: Simulated response to inter-annual SST variations in the Gulf Stream region. *Clim Dyn* **42,** 715–731.

Haney, S., B. Fox-Kemper, K. Julien, and A. Webb, 2015: Symmetric and geostrophic instabilities in the wave-forced ocean mixed layer. *J. Phys. Oceanogr.*, **45**, 3033–3056.

Harrison, C. S., M. C. Long, N. S. Lovenduski, and J. K. Moore, 2018: Mesoscale effects on carbon export: a global perspective. *Glob. Biogeochem. Cycles*, **32**, 680–703.

Hashizume, H., S.-P. Xie, M. Fujiwara, M. Shiotani, T. Watanabe, Y. Tanimoto, W. T. Liu, and K. Takeuchi, 2002: Direct observations of atmospheric boundary layer response to SST variations associated with tropical instability waves over the eastern equatorial Pacific. *J. Climate*, **15**, 3379–3393.

Hausmann, U., D. J. McGillicuddy, and J. Marshall, 2017: Observed mesoscale eddy signatures in Southern Ocean surface mixed-layer depth. *J. Geophys. Res. Oceans*, **122**, 617–635,

Hawcroft, M. K., L. C. Shaffrey, K. I. Hodges, and H. F. Dacre, 2012: How much Northern Hemisphere precipitation is associated with extratropical cyclones? *Geophys. Res. Lett.*, **39**, L24809.

Hayasaki, M., R. Kawamura, M. Mori, and M. Watanabe, 2013: Response of extratropical cyclone activity to the Kuroshio large meander in northern winter. *Geophys. Res. Lett.*, **40**, 2851–2855.

Hayes, S. P., M. J. McPhaden, and J. M. Wallace, 1989: The Influence of Sea Surface Temperature on Surface Wind in the Eastern Equatorial Pacific: Weekly to Monthly Variability. *J. Climate*, **2**, 1500-1506.

Hersbach, H., and Coauthors, 2020: The ERA5 global reanalysis. *Quart. J. Roy. Met. Soc.*, **146**, 1999-2049.

Hirata, H., R. Kawamura, M. Nonaka, and K. Tsuboki, 2019: Significant impact of heat supply from the Gulf Stream on a “superbomb” cyclone in January 2018. *Geophys. Res. Lett*, **46**, 7718–7725.

Hirata, H., and M. Nonaka, 2021: Impacts of strong warm ocean currents on development of extratropical cyclones through the warm and cold conveyor belts: A review. Elsevier, 9780128181577, 267-293 pp., doi:http://www.sciencedirect.com/science/article/pii/B9780128181560000149.

Hogg, A., W. K. Dewar, P. Berloff, S. Kravtsov, and D. K. Hutchinson, 2009: The effects of mesoscale ocean-atmosphere coupling on the large-scale ocean circulation. *J. Climate*, **22**, 4066-4082.

Holton, J. R., 1965a: The influence of viscous boundary layers on transient motions in a stratified rotating fluid. Part I. *J. Atmos. Sci*., **22**, 402–411.

Holton, J. R., 1965b: The influence of viscous boundary layers on transient motions in a stratified rotating fluid. Part II. *J. Atmos. Sci*., **22**, 535– 540.

Hoskins, B. J., and D. J. Karoly, 1981: The steady linear response of a spherical atmosphere to thermal and orographic forcing, *J. Atmos. Sci*., **38**, 1179-1196.

Hoskins, B. J., and K. I. Hodges, 2002: New Perspectives on the Northern Hemisphere Winter Storm Tracks. *J. Atmos. Sci.*, **59**, 1041–1061.

Hoskins, B. J., and P. J. Valdes, 1990: On the existence of storm tracks. *J. Atmos. Sci*., 47, 1854–1864.

Hotta, D., and H. Nakamura, 2011: On the significance of sensible heat supply from the ocean in the maintenance of mean baroclinicity along storm tracks. *J. Climate*, **24**, 3377–3401.

Infanti, J. M., and B. P. Kirtman, 2019: A comparison of CCSM4 high-resolution and low-resolution predictions for south Florida and southeast United States drought. *Clim. Dynm*., 52, 6877-6892.

IPCC, 2021: Climate Change 2021. The Physical Science Basis. Contribution of Working Group I to the Sixth Assessment Report of the Intergovernmental Panel on Climate Change [Masson-Delmotte, V., P. Zhai, A. Pirani, S.L. Connors, C. Péan, S. Berger, N. Caud, Y. Chen, L. Goldfarb, M.I. Gomis, M. Huang, K. Leitzell, E. Lonnoy, J.B.R. Matthews, T.K. Maycock, T. Waterfield, O. Yelekçi, R. Yu, and B. Zhou (eds.)]. Cambridge University Press. In Press.

Jackson, L. C., and Coauthors, 2020: Impact of ocean resolution and mean state on the rate of AMOC weakening. *Clim. Dyn.*, **55,** 1711–1732.

Jansen, M. F., and I. M. Held, 2014: Parameterizing subgrid-scale eddy effects using energetically consistent backscatter. *Ocean Modell.*, **80**, 36-48.

Johnson, L., C. M. Lee, and E. A. D'Asaro, 2016: Global Estimates of Lateral Springtime Restratification. *J. Phys. Oceanogr*., **46**, 1555-1573.

Jones, D. G., and Coauthors, 2015: Developments since 2005 in understanding potential environmental impacts of CO2 leakage from geological storage. *Int. J. Greenh. G. Con.*, **40**, 350–377.

Jullien, S., S. Masson, V. Oerder, G. Samson, F. Colas, and L. Renault, 2020: Impact of ocean-atmosphere current feedback on the ocean mesoscale activity: regional variations, and sensitivity to model resolution. *J. Climate*, **33**, 2585-2602.

Jury, M. R., and S. Courtney, 1991: A transition in weather over the Agulhas Current. *S. Afr. J. Mar. Sci.*, **10**, 159–171.

Karmalkar, A.V., and R. M. Horton, 2021: Drivers of exceptional coastal warming in the northeastern United States. *Nat. Clim. Chang.*, **11,** 854–860.

Kaspi, Y., and T. Schneider, 2013: The role of stationary eddies in shaping midlatitude storm tracks. *J. Atmos. Sci.*, **70**, 2596–2613.

Keil, P., and Coauthors, 2020: Multiple drivers of the North Atlantic warming hole. *Nat. Clim. Chang*., **10**, 667–671.

Kelly, K. A., S. Dickinson, M. J. McPhaden, and G. C. Johnson, 2001: Ocean Currents Evident in Satellite Wind Data. *Geophys. Res. Lett.*, **28**, 2469-2472.

Kelly, K. A., R. J. Small, R. M. Samelson, B. Qiu, T. M. Joyce, Y. Kwon, and M. F. Cronin, 2010: Western Boundary Currents and Frontal Air–Sea Interaction: Gulf Stream and Kuroshio Extension. *J. Climate*, **23**, 5644-5667.

Kessler, W.S., S. E. Wijffels, S. Cravatte, N. Smith, and Contributing Authors, 2019: Second Report of TPOS 2020. GOOS-234, 265 pp. [Available online at http://tpos2020.org/second-report/].

Kilpatrick, T., N. Schneider, and B. Qiu, 2014: Boundary layer convergence induced by strong winds across a midlatitude SST front. *J. Climate*, **27**, 1698–1718.

Kilpatrick, T., N. Schneider, and B. Qiu, 2016: Atmospheric response to a midlatitude SST front: Alongfront winds. *J. Atmos. Sci*., **73**, 3489–3509.

Kirincich, A., B. Emery, L. Washburn, and P. Flament, 2019: Improving Surface Current Resolution Using Direction Finding Algorithms for Multiantenna High-Frequency Radars, *J. Atmos. and Oceanic Technol*., **36**, 1997-2014.

Kirtman, B. P., and Coauthors, 2012: Impact of ocean model resolution on CCSM climate simulations. *Clim. Dyn*., **39**, 1303– 1328.

Kudryavtsev, V., B. Chapron, and V. Makin, 2014: Impact of wind waves on the air-sea fluxes: A coupled model. *J. Geophys. Res. Oceans*, **119**, 1217-1236.

Kushnir, Y., W. A. Robinson, I. Blade, N. M. J. Hall, S. Peng, and R. Sutton, 2002: Atmospheric GCM response to extratropical SST anomalies: Synthesis and evaluation. *J. Climate*, **15**, 2233-2256.

Kuwano-Yoshida, A., and S. Minobe, 2017. Storm track response to SST fronts in the Northwestern Pacific region in an AGCM. *J. Climate*, **30**, 1081-1102.

Kwak, K. H. Song, J. Marshall, H. Seo, and D. McGillicuddy, Jr., 2021: Suppressed pCO_2 in the Southern Ocean due to the interaction between current and wind. *J. Geophys. Res. Oceans*, https://doi.org/10.1029/2021JC017884.

Kwon, Y.-O., M. A. Alexander, N. A. Bond, C. Frankignoul, H. Nakamura, B. Qiu, and L. A. Thompson, 2010. Role of the Gulf Stream and Kuroshio-Oyashio Systems in Large-Scale Atmosphere-Ocean Interaction: A Review. *J. Climate*, **23**, 3249-3281.

Kwon, Y.-O., and T. M. Joyce, 2013: Northern Hemisphere Winter Atmospheric Transient Eddy Heat Fluxes and the Gulf Stream and Kuroshio-Oyashio Extension Variability. *J. Climate*, **26**, 9839-9859.

Lambaerts, J., G. Lapeyre, R. Plougonven, and P. Klein, 2013: Atmospheric response to sea surface temperature mesoscale structures. *J. Geophys. Res. Atmos*., **118**, 9611–9621.

Lac, C., and Coauthors, 2018: Overview of the Meso-NH model version 5.4 and its applications. *Geosci. Model Dev*., **11**, 1929-1969.

Lane, E. M., J. M. Restrepo, and J. C. McWilliams, 2007: Wave–current interaction: A comparison of radiation-stress and vortex-force representations. *J. Phys. Oceanogr*, **37**, 1122–1141.

Laurindo, L. C., A. Mariano, and R. Lumpkin, 2017: An improved surface velocity climatology for the global ocean from drifter observations. *Deep Sea Res. I*, **124**, 73–92.

Laurindo, L. C., L. Siqueira, A. J. Mariano, and B. Kirtman, 2019: Cross-spectral analysis of the SST/10-m wind speed coupling resolved by satellite products and climate model simulations. *Clim. Dyn*., **52**, 5071–5098.

Lee, R. W., T. J. Woollings, B. J. Hoskins, K. D. Williams, C. H. O'Reilly, and G. Masato, 2018: Impact of Gulf Stream SST biases on the global atmospheric circulation. *Clim Dyn.*, **51**, 3369–3387.

Leibovich, S., 1983: The Form and Dynamics of Langmuir Circulations. *Annu. Rev. Fluid Mech.*, **15**, 391-427.

Lenschow, D. H., P. B. Krummel, and S. T. Siems, 1999: Measuring Entrainment, Divergence, and Vorticity on the Mesoscale from Aircraft. *J. Atmos. Ocean Tech*., **16**, 1384-1400.

Lévy, M., 2008: The modulation of biological production by oceanic mesoscale turbulence. In *Transport and Mixing in Geophysical Flows*, ed. J Weiss, A Provenzale, pp. 219–61. Berlin: Springer

Lévy, M., P. J. S. Franks, and K. S. Smith, 2018: The role of submesoscale currents in structuring marine ecosystems. *Nat. Commun*., **9**, 4758.

Li, Y., and R. E. Carbone, 2012: Excitation of rainfall over the tropical western Pacific. *J. Atmos. Sci*., **69**, 2983–2994.

Lindzen, R. S., and B. Farrell, 1980: A Simple Approximate Result for the Maximum Growth Rate of Baroclinic Instabilities. *J. Atmos. Sci*., **37**, 1648-1654.

Lindzen, R. S., and S. Nigam, 1987: On the role of sea surface temperature gradients in forcing low-level winds and convergence in the tropics. *J. Atmos. Sci*., **44**, 2418–2436.

Liu, W., A. V. Fedorov, S.-P. Xie, and S. Hu, 2020: Climate impacts of a weakened Atlantic meridional overturning circulation in a warming climate. *Science Advances*, **6**, eaaz4876.

Liu, X., X. Ma, P. Chang, Y. Jia, D. Fu, G. Xu, L. Wu, R. Saravanan, and C. M. Patricola, 2021: Ocean fronts and eddies force atmospheric rivers and heavy precipitation in western North America. *Nat. Commun*., **12**, 1268.

López-Dekker, P., H. Rott, P. Prats-Iraola, B. Chapron, K. Scipal, and E. D. Witte, 2019: Harmony: an Earth Explorer 10 Mission Candidate to Observe Land, Ice, and Ocean

Surface Dynamics, in: IGARSS 2019 - 2019 IEEE International Geoscience and Remote Sensing Symposium, pp. 8381–8384, https://doi.org/10.1109/IGARSS.2019.8897983.

Lorenz, E., 1960: Generation of available potential energy and the intensity of the general circulation. In R. L. Pfeffer (Ed.), Dynamics of climate (pp. 86–92). Oxford: Pergamon Press.

Luo, J.-J., S. Masson, E. Roeckner, G. Madec, and T. Yamagata, 2005: Reducing Climatology Bias in an Ocean-Atmosphere CGCM with Improved Coupling Physics. *J. Climate,* **18**, 2344-2360

Ma, X., P. Chang, R. Saravanan, R. M. J.-S. Hseih, D. Wu, X. Lin, L. Wu, and Z. Jing, 2015: Distant influence of Kuroshio eddies on North Pacific weather patterns. *Sci. Rep*., **5**, 17785.

Ma, X., and Coauthors, 2016: Western boundary currents regulated by interaction between ocean eddies and the atmosphere. *Nature*, **535**, 533–537.

Ma, X., P. Chang, R. Saravanan, R. Montuoro, H. Nakamura, D. Wu, X. Lin, and L. Wu, 2017: Importance of resolving Kuroshio Front and eddy influence in simulating the North Pacific storm track. *J. Climate,* **30**, 1861-1880.

Mahrt, L., D. Vickers, and E. Moore, 2004: Flow Adjustments Across Sea-Surface Temperature Changes. *Boundary-Layer Meteorology* **111,** 553–564.

Marshall, J., and Coauthors, 2009: The Climode Field Campaign: Observing the Cycle of Convection and Restratification over the Gulf Stream. *Bull. Amer. Meteor. Soc.*, **90**, 1337–1350.

Marshall, J., J. Scott, K. Armour, J.-M. Campin, M. Kelley, and A. Romanou, 2014: The ocean's role in the transient response of climate to abrupt greenhouse gas forcing. *Clim. Dyn*., **44,** 2287–2299.

Martin, A., and K. Richards, 2001: Mechanisms for vertical nutrient transport within a North Atlantic mesoscale eddy. *Deep Sea Res.–II*, **48**, 757–773.

Masunaga, R., H. Nakamura, B. Taguchi and T. Miyasaka, 2020a: Processes Shaping the Frontal-Scale Time-Mean Surface Wind Convergence Patterns around the Kuroshio Extension in Winter. *J. Climate,* **33**, 3-25.

Masunaga, R., H. Nakamura, B. Taguchi, and T. Miyasaka, 2020b: Processes Shaping the Frontal-Scale Time-Mean Surface Wind Convergence Patterns around the Gulf Stream and Agulhas Return Current in Winter. *J. Climate*, **33**, 9083–9101.

Masunaga, R. and N. Schneider, 2021: Surface wind responses to mesoscale sea surface temperature over western boundary current regions assessed by spectral transfer functions. *J. Atmos. Sci*., submitted.

McGillicuddy, D. J., and Coauthors, 2007: Eddy/Wind Interactions Stimulate Extraordinary Mid-Ocean Plankton Blooms. *Science*, **316**, 1201.

McGillicuddy, D. J., 2016: Mechanisms of physical-biological-biogeochemical interaction at the oceanic mesoscale. *Ann. Rev. Mar. Sci.*, **8**, 125-159.

McGillis, W. R., J. B. Edson, J. E. Hare, and C. W. Fairall, 2001: Direct covariance air-sea CO2 fluxes. *J. Geophys. Res.*, **106**, 16729-16745.

McLandress, C., T. Shepherd, J. Scinocca, D. Plummer, M. Sigmond, A. Jonsson, and M. Reader, 2011: Separating the dynamical effects of climate change and ozone depletion. Part II: Southern hemisphere troposphere. *J. Climate*, **24**, 1850–1868.

McWilliams, J. C., E. Huckle, J. Liang, and P. P. Sullivan, 2012: The Wavy Ekman Layer: Langmuir Circulations, Breaking Waves, and Reynolds Stress. *J. Phys. Oceanogr*., **42**, 1793-1816.

McWilliams, J. C., and B. Fox-Kemper, 2013: Oceanic wave-balanced surface fronts and filaments. *J. Fluid Mech*., **730**, 464-490.

Meinig, C., and Coauthors, 2019: Public-Private Partnerships to Advance Regional Ocean-Observing Capabilities: A Saildrone and NOAA-PMEL Case Study and Future Considerations to Expand to Global Scale Observing. *Front. Mar. Sci.*, **6**, 448.

Mémin, E. 2014: Fluid flow dynamics under location uncertainty. *Geophysical & Astrophysical Fluid Dynamics*, **108**, 119-146.

Menary, M. B., and Coauthors, 2018: Preindustrial control simulations with HadGEM3-GC3.1 for CMIP6. *J. Adv. Model. Earth Syst.*, **10**, 3049– 3075.

Messager, C., and S. Swart, 2016: Significant atmospheric boundary layer change observed above an Agulhas Current warm core eddy. *Adv. Meteor*., 2016, 3659657.

Mey, R. D., N. D. Walker, and M. R. Jury, 1990: Surface heat fluxes and marine boundary layer modification in the Agulhas Retroflection Region. *J. Geophys. Res.*, **95,** 15 997–16 015.

Minobe, S., A. Kuwano-Yoshida, N. Komori, S.-P. Xie, and R. J. Small, 2008: Influence of the Gulf Stream on the troposphere. *Nature*, **452**, 206–209.

Minobe, S., M. Miyashita, A. Kuwano-Yoshida, H. Tokinaga, and S.-P. Xie, 2010: Atmospheric response to the Gulf Stream: Seasonal variations. *J. Climate*, **23**, 3699–3719.

Moreno-Chamarro, E., L.-P. Caron, P. Ortega, S. Loosveldt Tomas, and M. J. Roberts, 2021: Can we trust CMIP5/6 future projections of European winter precipitation? *Environ. Res. Lett.*, **16**, 054063.

Moreton, S., D. Ferreira, M. Roberts, and H. Hewitt, 2021: Air-Sea Turbulent Heat Flux Feedback over Mesoscale Eddies. *Geophys. Res. Lett*., **48**, e2021GL095407.

Nadiga, B. T., 2008: Orientation of eddy fluxes in geostrophic turbulence. *Phil. Trans. R. Soc. A.*, **366,** 2489-2508.

Nakamura H., T. Sampe, Y. Tanimoto, and A. Shimpo, 2004: Observed associations among storm tracks, jet streams and midlatitude oceanic fronts. "Earth's climate: the ocean-atmosphere interaction". *AGU Geophys Monogr.,* **147**, 329–346.

Nakamura, H., T. Sampe, A. Goto, W. Ohfuchi, and S.-P. Xie, 2008: On the importance of midlatitude oceanic frontal zones for the mean state and dominant variability in the tropospheric circulation. *Geophys. Res. Lett.*, **35**, L15709.

Nakamura, H., and A. Shimpo, 2004: Seasonal Variations in the Southern Hemisphere Storm Tracks and Jet Streams as Revealed in a Reanalysis Dataset. *J. Climate*, **17**, 1828–1844.

Nakamura, H., A. Nishina, and S. Minobe, 2012: Response of storm tracks to bimodal Kuroshio path states south of Japan. *J. Climate*, **25**, 7772–7779.

Nakamura, H., and Coauthors, 2015: "Hot Spots" in the climate system—new developments in the extratropical ocean-atmosphere interaction research: a short review and an introduction. *J. Oceanogr.*, **71**, 463–467.

Nakayama, M., H. Nakamura, and F. Ogawa, 2021: Impacts of a Midlatitude Oceanic Frontal Zone for the Baroclinic Annular Mode in the Southern Hemisphere. *J. Climate*, **34**, 7389-7408.

Nkwinkwa Njouodo, A. S., S. Koseki, N. Keenlyside, and M. Rouault, 2018: Atmospheric signature of the Agulhas Current. *Geophys. Res. Lett.*, **45**, 5185–5193.

Nonaka, M., H. Nakamura, B. Taguchi, N. Komori, A. Yoshida-Kuwano, and K. Takaya, 2009: Air-sea heat exchanges characteristic to a prominent

midlatitude oceanic front in the South Indian Ocean as simulated in a high-resolution coupled GCM. *J. Climate*, **22**, 6515–6535.

Omand, M. M., E. A. D'Asaro, C. M. Lee, M.-J. Perry, N. Briggs, I. Cetinić, and A. Mahadevan, 2015: Eddy-driven subduction exports particulate organic carbon from the spring bloom. *Science*, **348**, 222-225.

Olivier, L., and Coauthors, 2021: Impact of North Brazil Current rings on air-sea CO2 flux variability in winter 2020. *Biogeosciences*, https://doi.org/10.5194/bg-2021-269.

O'Neill, L. W., D. B. Chelton, and S. K. Esbensen, 2003: Observations of SST-induced perturbations of the wind stress field over the Southern Ocean on seasonal timescales. *J. Climate*, **16**, 2340– 2354.

O'Neill, L. W., D. B. Chelton, and S. K. Esbensen, 2010: The effects of SST-induced wind speed and direction gradients on mid-latitude surface vorticity and divergence. *J. Climate*, **23**, 255-281.

O'Neill, L. W., D. B. Chelton, and S. K. Esbensen, 2012: Covariability of surface wind and stress responses to sea surface temperature fronts. *J. Climate*, **25**, 5916–5942.

O'Neill, L. W., 2012: Wind Speed and Stability Effects on Coupling between Surface Wind Stress and SST Observed from Buoys and Satellites. *J. Climate, **25***, 1544-1569.

O'Neill, L. W., T. Haack, and T. Durland, 2015: Estimation of time-averaged surface divergence and vorticity from satellite ocean vector winds. *J. Climate*, **28**, 7596–7620.

O'Neill, L. W., T. Haack, D. B. Chelton, and E. D. Skyllingstad, 2017: The Gulf Stream Convergence Zone in the time-mean winds. *J. Atmos. Sci*., **74**, 2383-2412.

O'Reilly, C. H., and A. Czaja, 2015: The response of the Pacific storm track and atmospheric circulation to Kuroshio Extension variability. *Quart. J. Roy. Met. Soc*., **141**, 52–66.

O'Reilly, C. H., S. Minobe, and A. Kuwano-Yoshida, 2016: The influence of the Gulf Stream on wintertime European blocking. *Clim. Dyn.*, **47**, 1545–1567.

O'Reilly, C. H., S. Minobe, A. Kuwano-Yoshida, and T. Woollings, 2017: The Gulf Stream influence on wintertime North Atlantic jet variability. *Quart. J. Roy. Meteor. Soc*., **143**, 173–183.

Pacanowski, R. C., 1987: Effect of Equatorial Currents on Surface Stress. *J. Phys. Oceanogr*., **17**, 833-838.

Paduan, J. D., and L. Washburn, 2013: High-Frequency Radar Observations of Ocean Surface Currents. *Ann. Rev. Mar. Sci.,* **5**, 115-136.

Palmer, T. N., and Z. Sun, 1985: A modeling and observational study of the relationship between sea-surface temperature in the northwest Atlantic and the atmospheric general circulation, *Quart. J. Roy. Meteor. Soc*., **111**, 947-975.

Parfitt, R., A. Czaja, S. Minobe, and A. Kuwano-Yoshida, 2016: The atmospheric frontal response to SST perturbations in the Gulf Stream region. *Geophys. Res. Lett*., **43**, 2299–2306.

Parfitt, R., and A. Czaja, 2016: On the contribution of synoptic transients to the mean atmospheric state in the Gulf Stream region. *Quart. J. Roy. Met. Soc.*, **142**, 1554–1561.

Parfitt, R., and H. Seo, 2018: A New Framework for Near-Surface Wind Convergence over the Kuroshio Extension and Gulf Stream in Wintertime: The Role of Atmospheric Fronts. *Geophys. Res. Lett*., **45**, 9909–9918.

Peng, S., A. Robinson, and M. P. Hoerling, 1997: The modeled atmospheric response to midlatitude SST anomalies and its dependence on background circulation states. *J. Climate*, **10**, 971–987.

Penny, S. G., and T. Hamill, 2017: Coupled data assimilation for integrated Earth system analysis and prediction. *Bull. Amer. Meteor. Soc*, **97**, ES169–ES172.

Perlin, N., S. P. de Szoeke, D. B. Chelton, R. M. Samelson, E. D. Skyllingstad, and L. W. O'Neill, 2014: Modeling the Atmospheric Boundary Layer Wind Response to Mesoscale Sea Surface Temperature Perturbations. *Mon. Wea. Rev.*, **142**, 4284–4307.

Pezzi, L. P., R. B. Souza, M. S. Dourado, C. A. E. Garcia, M. M. Mata, and M. A. F. Silva-Dias, 2005: Ocean-atmosphere in situ observations at the Brazil-Malvinas Confluence region. *Geophys. Res. Lett*., **32**, L22603.

Pezzi, L. P., and Coauthors, 2021*:* Oceanic eddy-induced modifications to air-sea heat and CO_2 fluxes in the Brazil-Malvinas Confluence. *Sci. Rep.*, **11**, 10648.

Piazza, M., L. Terray, J. Boé, E. Maisonnave, and E. Sanchez- Gomez, 2016: Influence of small-scale North Atlantic sea surface temperature patterns on the marine boundary layer and free troposphere: A study using the atmospheric ARPEGE model. *Climate Dyn*., **46**, 1699–1717.

Plagge, A. M., D. Vandemark, and B. Chapron, 2012: Examining the Impact of Surface Currents on Satellite Scatterometer and Altimeter Ocean Winds. *J. Atmos. Oceanic Tech.*, **29**, 1776-1793.

Polvani, L. M., D. W. Waugh, G. J. P. Correa, and S. Son, 2011: Stratospheric ozone depletion: The main driver of 20th century atmospheric circulation changes in the southern hemisphere, *J. Climate*, **24**, 795–812.

Polverari, F., M. Portabella, W. Lin, J. W. Sapp, A. Stoffelen, Z. Jelenak, and P. S. Chang, 2021: On High and Extreme Wind Calibration Using ASCAT. *IEEE Trans. Geosci. Remote Sens.*, 0.1109/TGRS.2021.3079898

Quinn, P. K., and Coauthors, 2021: Measurements from the RV Ronald H. Brown and related platforms as part of the Atlantic Tradewind Ocean-Atmosphere Mesoscale Interaction Campaign (ATOMIC). *Earth Syst. Sci. Data*, **13**, 1759–1790.

Reason, C. J. C., 2001: Evidence for the influence of the Agulhas Current on regional atmospheric circulation patterns. *J. Climate*, **14**, 2769–2778.

Reichl, B. G., and Deike, L., 2020: Contribution of sea-state dependent bubbles to air-sea carbon dioxide fluxes. *Geophys. Res. Lett.*, **47**, e2020GL087267.

Reeder, M. J., T. Spengler, and C. Spensberger, 2021: The Effect of Sea Surface Temperature Fronts on Atmospheric Frontogenesis. *J. Atmos. Sci*., **78**, 1753-1771.

Renault, L., J. C. McWilliams, A. F. Shchepetkin, F. Lemarié, D. Chelton, S. Illig, and A. Hall, 2016a: Modulation of wind work by oceanic current interaction with the atmosphere. *J. Phys. Oceanogr.*, **46**, 1685–1704.

Renault, L., M. J. Molemaker, J. Gula, S. Masson, and J. C. McWilliams, 2016b: Control and stabilization of the Gulf Stream by oceanic current interaction with the atmosphere. *J. Phys. Oceanogr*., **46**, 3439–3453.

Renault, L., J. C. McWilliams, and P. Penven, 2017a: Modulation of the Agulhas Current retroflection and leakage by oceanic current interaction with the atmosphere in coupled simulations. *J. Phys. Oceanogr*, **47**, 2077–2100.

Renault, L., J. C. McWilliams, and S. Masson, 2017b: Satellite observations of imprint of oceanic current on wind stress by air-sea coupling. *Sci. Rep.*, **7**, 17747.

Renault, L., J. C. McWilliams, and J. Gula, 2018: Dampening of submesoscale currents by air-sea stress coupling in the Californian upwelling system. *Sci. Rep.*, **8**, 13388.

Renault, L., S. Masson, V. Oerder, S. Jullien, and F. Colas, 2019a: Disentangling the mesoscale ocean-atmosphere interactions. *J. Geophys. Res. Oceans*, **124**, 2164–2178.

Renault, L., P. Marchesiello, S. Masson, and J. C. McWilliams, 2019b: Remarkable control of western boundary currents by eddy killing, a mechanical air-sea coupling process. *Geophys. Res. Lett.*, **46**, 2743–2751.

Renault, L., S. Masson, T. Arsouze, G. Madec, and J. C. McWilliams, 2020: Recipes for how to force oceanic model dynamics. *J. Adv. Modeling Earth Syst.*, **12**, e2019MS001715.

Renault L., S. Masson, V. Oerder, F. Colas, and J.C. McWilliams, Modulation of the Oceanic Mesoscale Activity by the Mesoscale Thermal FeedBack, *In preparation*.

Roberts, M. J., Hewitt, H. T., Hyder, P., Ferreira, D., Josey, S. A., Mizielinski, M., and Shelly, A., 2016: Impact of ocean resolution on coupled air-sea fluxes and large-scale climate, *Geophys. Res. Lett.*, **43**, 10,430– 10,438.

Robinson, W., P. Chang, E. Chassignet, and S. Speich, 2020: *Ocean Mesoscale Eddy Interactions with the Atmosphere* (No. 2020-05). (J. Zhu and M. Patterson, Eds.). Washington, DC: U.S. CLIVAR Project Office. doi:10.5065/ebjm-5q77.

Robinson, W., S. Speich, and E. Chassignet, 2018: Exploring the interplay between ocean eddies and the atmosphere, *Eos*, **99**, https://doi.org/10.1029/2018EO100609.

Romero, L., D. Hypolite, and J. C. McWilliams, 2020: Submesoscale current effects on surface waves. *Ocean Modell.*, **153**, 101662.

Rousseau, V., E. Sanchez-Gomez, R. Msadek, and M. Moine, 2021: Mechanisms shaping wind convergence under extreme synoptic situations over the Gulf Stream region. *J. Climate*, **34**, 9481-9500.

Saba, V. S., and Coauthors, 2016: Enhanced warming of the Northwest Atlantic Ocean under climate change. *J. Geophys. Res. Oceans*, **121**, 118-132.

Samelson R., E. Skyllingstad, D. Chelton, S. Esbensen, L. O'Neill, and N. Thum, 2006: On the coupling of wind stress and sea surface temperature. *J. Climate*, **19**, 1557-1566.

Samelson, R. M., L. W. O'Neill, D. B. Chelton, E. D. Skyllingstad, P. L. Barbour, and S. M. Durski, 2020: Surface Stress and Atmospheric Boundary Layer Response to Mesoscale SST Structure in Coupled Simulations of the Northern California Current System. *Mon. Wea. Rev.*, **148**, 259-287.

Sampe, T., and S.-P. Xie, 2007: Mapping high sea winds from space: A global climatology. *Bull. Amer. Meteor. Soc.*, **88**, 1965-1978.

Saviano, S., and Coauthors, 2021: Wind Direction Data from a Coastal HF Radar System in the Gulf of Naples (Central Mediterranean Sea, *Remote Sens*., **13**, 1333.

Schneider, N., and B. Qiu, 2015: The atmospheric response to weak sea surface temperature fronts. *J. Atmos. Sci.,* **72**, 3356–3377.

Schneider, N., 2020: Scale and Rossby Number Dependence of Observed Wind Responses to Ocean-Mesoscale Sea Surface Temperatures. *J. Climate*, **77**, 3171-3192.

Scott, R. B., and Y. Xu, 2009: An update on the wind power input to the surface geostrophic flow of the World Ocean. *Deep-Sea Res.*, **56**, 295–304.

Seager, R., Y. Kushnir, N. H. Naik, M. A. Cane, and J. Miller, 2001: Wind-Driven Shifts in the Latitude of the Kuroshio–Oyashio Extension and Generation of SST Anomalies on Decadal Timescales. *J. Climate*, **14**, 4249-4265.

Seager, R., and I. R. Simpson, 2016: Western boundary currents and climate change. *J. Geophys. Res. Oceans*, **121**, 7212–7214.

Seo, H., M. Jochum, R. Murtugudde, A. J. Miller, and J. O. Roads, 2007: Feedback of Tropical Instability Wave - induced Atmospheric Variability onto the Ocean. *J. Climate,* **20**, 5842-5855.

Seo, H., Y.-O. Kwon, and J.-J. Park, 2014: On the effect of the East/Japan Sea SST variability on the North Pacific atmospheric circulation in a regional climate model. *J. Geophys. Res. Atmos*., **119**, 418–444.

Seo, H., A. J. Miller, and J. R. Norris, 2016: Eddy-wind interaction in the California Current System: dynamics and impacts. *J. Phys. Oceanogr*., **46**, 439-459.

Seo, H., 2017: Distinct influence of air-sea interactions mediated by mesoscale sea surface temperature and surface current in the Arabian Sea. *J. Climate,* **30**, 8061-8079.

Seo, H., Y.-O. Kwon, T. M. Joyce, and C. C. Ummenhofer, 2017: On the predominant nonlinear response of the extratropical atmosphere to meridional shift of the Gulf Stream. *J. Climate,* **30**, 9679-9702.

Seo, H., A. C. Subramanian, H. Song, and J. S. Chowdary, 2019: Coupled effects of ocean current on wind stress in the Bay of Bengal: Eddy energetics and upper ocean stratification. *Deep-Sea Res. II*, **168**, 104617.

Seo, H., H. Song, L. W. O'Neill, M. R. Mazloff, and B. D. Cornuelle, 2021: Impacts of ocean currents on the South Indian Ocean extratropical storm track through the relative wind effect. *J. Climate,* **34**, 9093-9113.

Sheldon, L., A. Czaja, B. Vannière, C. Morcrette, B. Sohet, M. Casado, and D. Smith, 2017: A warm path to Gulf Stream–troposphere interactions. *Tellus*, **69**, 1–13.

Shi, Q., and M. A. Bourassa, 2019: Coupling Ocean Currents and Waves with Wind Stress over the Gulf Stream. *Remote Sens*., **11**, 1476.

Shinoda, T., S. Pei, W. Wang, J. X. Fu. R.-C. Lien, H. Seo, and A. Soloviev, 2021: Climate Process Team: improvement of ocean component of NOAA Climate Forecast System relevant to Madden-Julian Oscillation simulations. *J. Adv. Model. Earth Syst.,* **13**, e2021MS002658.

Shroyer, E., and Coauthors, 2021: Bay of Bengal Intraseasonal Oscillation and the 2018 Monsoon Onset. *Bull. Amer. Meteo. Soc.,* **102**, E1936-E1951.

Singleton, A. T., and C. J. C. Reason, 2006: Numerical simulations of a severe rainfall event over the Eastern Cape coast of South Africa: Sensitivity to sea surface temperature and topography. *Tellus,* **58A**, 335–367.

Siqueira, L., and B. P. Kirtman, 2016: Atlantic near-term climate variability and the role of a resolved Gulf Stream. *Geophys. Res. Lett*., **43**, 3964–3972.

Siqueira, L., B. P. Kirtman, and L. C. Laurindo, 2021: Forecasting Remote Atmospheric Responses to Decadal Kuroshio Stability Transitions. *J. Climate,* **34**, 379–395.

Skyllingstad, E. D., D. Vickers, L. Mahrt, and R. Samelson, 2007: Effects of mesoscale sea-surface temperature fronts on the marine atmospheric boundary layer. *Boundary-Layer Meteorol,* **123,** 219–237.

Skyllingstad, E. D., and J. B. Edson, 2009: Large-eddy simulation of moist convection during a cold-air outbreak over the Gulf Stream. *J. Atmos. Sci.,* **66**(5), 1274-1293.

Skyllingstad, E. D., S. P. de Szoeke, and L. W. O'Neill, 2019: Modeling the Transient Response of Tropical Convection to Mesoscale SST Variations. *J. Atmos. Sci.*, **76**, 1227-1244.

Small, R. J., S.-P. Xie, Y. Wang, S. K. Esbensen, and D. Vickers, 2005a: Numerical Simulation of Boundary Layer Structure and Cross-Equatorial Flow in the Eastern Pacific. *J. Atmos. Sci.*, **62**(6), 1812-1830.

Small, R. J., S.-P. Xie, and J. Hafner, 2005b: Satellite observations of mesoscale ocean features and copropagating atmospheric surface fields in the tropical belt. *J. Geophys. Res*., **110**, C02021.

Small, R. J., S. de Szoeke, S.-P. Xie, L. O'Neill, H. Seo, Q. Song, P. Cornillon, M. Spall, and S. Minobe, 2008: Air-Sea Interaction over Ocean Fronts and Eddies. *Dyn. Atmos. Oceans*, **45**, 274-319.

Small, R. J., R. Msadek, Y. Kwon, J. F. Booth, and C. Zarzycki, 2019: Atmosphere surface storm track response to resolved ocean mesoscale in two sets of global climate model experiments. *Clim. Dyn.*, **52**, 2067–2089.

Smirnov, D., M. Newman, M. A. Alexander, Y.-O. Kwon, and C. Frankignoul, 2015: Investigating the local atmospheric response to a realistic shift in the Oyashio sea surface temperature front. *J. Climate*, **28**, 1126–1147.

Song, H., J. Marshall, P. Gaube, and D. J. McGillicuddy, 2015: Anomalous chlorofluorocarbon uptake by mesoscale eddies in the Drake Passage region. *J. Geophys. Res. Oceans*, **120**, 1065-1078.

Song, H., J. Marshall, M. J. Follows, S. Dutkiewicz and G. Forget, 2016: Source waters for the highly productive Patagonian shelf in the southwestern Atlantic. *J. Mar. Syst.*, **158**, 120-128.

Song, Q., P. Cornillon, and T. Hara, 2006: Surface wind response to oceanic fronts. *J. Geophys. Res*., **111**, C12006.

Song, Q., D. B. Chelton, S. K. Esbensen, N. Thum, and L. W. O'Neill, 2009: Coupling between Sea Surface Temperature and Low-Level Winds in Mesoscale Numerical Models. *J. Climate*, **22**, 146-164.

Song, Q., D. B. Chelton, S. K. Esbensen, and A. R. Brown, 2017: An Investigation of the Stability Dependence of SST-Induced Vertical Mixing over the Ocean in the Operational Met Office Model. *J. Climate*, **30**, 91-107.

Song, H., J. Marshall, D. J. McGillicuddy Jr., and H. Seo, 2020: The impact of the current-wind interaction on the vertical processes in the Southern Ocean. *J. Geophys. Res.-Oceans*, **125**, e2020JC016046.

Souza, R., L. Pezzi, S. Swart, F. Oliveira, and M. Santini, 2021: Air-Sea Interactions over Eddies in the Brazil-Malvinas Confluence. *Remote Sens.*, **13**, 1335.

Spall, M. A., 2007: Effect of sea surface temperature-wind stress coupling on baroclinic instability in the ocean. *J. Phys. Oceanogr*., **37**, 1092-1097.

Sprintall, J., V. J. Coles, K. A. Reed, A. H. Butler, G. R. Foltz, S. G. Penny, and H. Seo, 2020: Best practice strategies for process studies designed to improve climate modeling. *Bull. Amer. Meteor. Soc.*, **101**, E1842–1850.

Stevens, B., and Coauthors, 2003: Dynamics and Chemistry of Marine Stratocumulus – DYCOMS-II. *Bull. Amer. Meteor. Soc*., **84**, 579–594.

Stevens, B., and Coauthors, 2019: DYAMOND: the DYnamics of the Atmospheric general circulation modeled on non-hydrostatic domains. *Prog. Earth Planet Sci*., **6,** 61.

Stevens, B., and Coauthors, 2021: EUREC4A. *Earth System Science Data*, **13**, 4067-4119.

Stoffelen, A., R. Kumar, J. Zou, V. Karaev, P. S. Chang, and E. Rodriguez, 2019: Ocean Surface Vector Wind Observations. In: Barale V., Gade M. (eds) Remote Sensing of the Asian Seas. Springer, Cham. https://doi.org/10.1007/978-3-319-94067-0_24.

Su, Z., and Coauthors, 2018: Ocean submesoscales as a key component of the global heat budget. *Nat. Commun.*, **9**, 775.

Sugimoto, S., B. Qiu, and N. Schneider, 2021: Local Atmospheric Response to the Kuroshio Large Meander Path in Summer and Its Remote Influence on the Climate of Japan. *J. Climate*, **34**, 3571-3589.

Sullivan, P., and J. C. McWilliams, 2019: Langmuir turbulence and filament frontogenesis in the oceanic surface boundary layer. *J. Fluid Mech*., **879**, 512-553.

Sullivan, P. P., J. C. McWilliams, J. C. Weil, E. G. Patton, and H. J. S. Fernando, 2020: Marine Boundary Layers above Heterogeneous SST: Across-Front Winds. *J. Atmos. Sci*., **77**, 4251-4275.

Sullivan, P. P., J. C. McWilliams, J. C. Weil, E. G. Patton, and H. J. S. Fernando, 2021: Marine Boundary Layers above Heterogeneous SST: Alongfront Winds. *J. Atmos. Sci*., **78**, 3297-3315.

Sun, X., and R. Wu, 2021: Spatial scale dependence of the relationship between turbulent surface heat flux and SST. *Clim. Dyn.*, https://doi.org/10.1007/s00382-021-05957-9.

Suzuki, N., B. Fox-Kemper, P. E. Hamlington, and L. P. Van Roekel, 2016: Surface waves affect frontogenesis. *J. Geophys. Res. Oceans*, **121**, 1-28.

Sweet, W., R. Fett, J. Kerling, and P. La Violette, 1981: Air-sea interaction effects in the lower troposphere across the north wall of the Gulf Stream. *Mon. Wea. Rev*., **109**, 1042–1052.

Taguchi, B., S.-P. Xie, N. Schneider, M. Nonaka, H. Sasaki, and Y. Sasai, 2007: Decadal variability of the Kuroshio Extension: Observations and an eddy-resolving model hindcast. *J. Climate*, **20**, 2357–2377.

Taguchi, B., H. Nakamura, M., Nonaka, K. Komori, A. Kuwano-Yoshida, K. Takaya, and A. Goto, 2012: Seasonal evolutions of atmospheric response to decadal SST anomalies in the North Pacific subarctic frontal zone: observations and a coupled model simulation. *J. Climate*, **25**, 111–139.

Takatama, K., S. Minobe, M. Inatsu, and R. J. Small, 2012: Diagnostics for near-surface wind convergence/divergence response to the Gulf Stream in a regional atmospheric model. *Atmos. Sci. Lett*., **13**, 16–21.

Takatama, K., S. Minobe, M. Inatsu, and R. J. Small, 2015: Diagnostics for near-surface wind response to the Gulf Stream in a regional atmospheric model. *J. Climate*, **28**, 238–255.

Takatama, K., and N. Schneider, 2017: The Role of Back Pressure in the Atmospheric Response to Surface Stress Induced by the Kuroshio. *J. Atmos. Sci.*, **74**, 597–615.

Thomson, J., 2012: Wave Breaking Dissipation Observed with "SWIFT" Drifters. *J. Atmos. Oceanic Technol*., **29**, 1866-1882.

Thomson, J., and J. Girton, 2017: Sustained measurements of Southern Ocean air-sea coupling from a Wave Glider autonomous surface vehicle. *Oceanogr*., **30**, 104–109.

Thum, N., S. K. Esbensen, D. B. Chelton, and M. J. McPhaden, 2002: Air-sea heat exchange along the northern sea surface temperature front in the eastern tropical Pacific. *J. Climate*, **15**, 3361–3378.

Tokinaga, H., Y. Tanimoto, and S.-P. Xie, 2005: SST-Induced Surface Wind Variations over the Brazil–Malvinas Confluence: Satellite and In Situ Observations. *J. Climate*, **18**, 3470-3482.

Trenberth, K. E., and D. J. Shea, 2005: Relationships between precipitation and surface temperature. *Geophys. Res. Lett*., **32**, L14703.

Tokinaga, H., Y. Tanimoto, S.-P. Xie, T. Sampe, H. Tomita, and H. Ichikawa, 2009: Ocean Frontal Effects on the Vertical Development of Clouds over the Western North Pacific: In Situ and Satellite Observations. *J. Climate*, **22**, 4241-4260.

Trindade, A., M. Portabella, A. Stoffelen, W. Lin, and A. Verhoef, 2020: ERAstar: A High-Resolution Ocean Forcing Product. *IEEE Transactions on Geoscience and Remote Sensing*, **58**, 1337–1347.

Trowbridge, J., R. Weller, D. Kelley, E. Dever, A. Plueddemann, J. A. Barth, and O. Kawka, 2019: The Ocean Observatories Initiative. *Front. Mar. Sci.*, **6**, 74.

Tsopouridis, L., C. Spensberger, and T. Spengler, 2021: Cyclone intensification in the Kuroshio region and its relation to the sea surface temperature front and upper-level forcing. *Quart. J. Roy. Met. Soc*., **147**, 485-500.

Vannière, B., A. C. H. Dacre, and T. Woollings, 2017: A "cold path" for the Gulf Stream–troposphere connection. *J. Climate*, **30**, 1363–1379.

Vecchi, G. A., S.-P. Xie, and A. S. Fischer, 2004: Ocean-atmosphere covariability in the western Arabian Sea. *J. Climate*, **17**, 1213-1224.

Verdy, A., and M. R. Mazloff, 2017: A data assimilating model for estimating Southern Ocean biogeochemistry. *J. Geophys. Res. Oceans*, **122**, 6968– 6988.

Villas Bôas, A. B., O. T. Sato, A. Chaigneau, and G. P. Castelão, 2015: The signature of mesoscale eddies on the air-sea turbulent heat fluxes in the South Atlantic Ocean. *Geophys. Res. Lett.*, **42**, 1856–1862.

Villas Bôas, A. B., and Coauthors, 2019: Integrated Observations of Global Surface Winds, Currents, and Waves: Requirements and Challenges for the Next Decade. *Front. Mar. Sci*., **6**, 425.

Villas Bôas, A. B., and W. Young, 2020: Directional diffusion of surface gravity wave action by ocean macroturbulence. *J. Fluid Mech*., **890**, R3.

Villas Bôas, A. B., B. D. Cornuelle, M. R. Mazloff, S. T. Gille, and F. Ardhuin, 2020: Wave–Current Interactions at Meso- and Submesoscales: Insights from Idealized Numerical Simulations. *J. Phys. Oceanogr*., **50**, 3483-3500.

Villas Bôas, A. B., and N. Pizzo, 2021: The geometry, kinematics, and dynamics of the two-way coupling between wind, waves, and currents. *US CLIVAR Variations*, **19**, 18-26.

Wai, M. M., and S. A. Stage, 1989: Dynamical analyses of marine atmospheric boundary layer structure near the Gulf Stream oceanic front. *Quart. J. Roy. Met. Soc.*, **115**, 29–44.

Wallace, J. M., T. P. Mitchell, and C. Deser, 1989: The influence of sea surface temperature on sea surface wind in the eastern equatorial Pacific. Seasonal and interannual variability. *J. Climate*, **2**, 1492–1499.

Wang, Y., C. Wang, H. Zhang, Y. Dong, and S. Wei, 2019: SAR Dataset of Ship Detection for Deep Learning under Complex Backgrounds. *Remote Sens*., **11**, 765.

Wang, Q., J. A. Kalogiros, S. R. Ramp, J. D. Paduan, G. Buzorius, and H. Jonsson, 2011: Wind Stress Curl and Coastal Upwelling in the Area of Monterey Bay Observed during AOSN-II. *J. Phys. Oceanogr*., **41**, 857–877.

Wang, Q., and Coauthors, 2018: CASPER: Coupled Air-Sea Processes and Electromagnetic (EM) ducting Research. *Bull. Amer. Meteor. Soc*., **99**, 1449–1471.

Wanninkhof, R., 1992: Relationship between wind speed and gas exchange over the ocean. *J. Geophys. Res.*, **97**, 7373–7382.

Wanninkhof, R., W. E. Asher, D. T. Ho, C. Sweeney, and W. R. McGillis, 2009: Advances in quantifying air-sea gas exchange and environmental forcing. *Ann. Rev. Mar. Sci.*, **1**, 213–44.

Wanninkhof, R., G. Park, D. B. Chelton, and C. M. Risien, 2011: Impact of Small-Scale Variability on Air-Sea CO_2 Fluxes. In Gas Transfer at Water Surfaces, 2010, edited by S. Komori, W. McGillis, and R. Kurose, 431–44. Kyoto University Press, Kyoto.

Warner, T. T., M. N. Lakhtakia, J. D. Doyle, and R. A. Pearson, 1990: Marine atmospheric boundary layer circulations forced by Gulf Stream sea surface temperature gradients. *Mon. Wea. Rev*., **118**, 309–323.

Weaver, A. J., Coauthors, 2012: Stability of the Atlantic meridional overturning circulation: A model intercomparison. *Geophys. Res. Lett.*, **39**, L20709.

Wenegrat, J. O., and R. S. Arthur, 2018: Response of the atmospheric boundary layer to submesoscale sea surface temperature fronts. *Geophys. Res. Lett.*, **45**, 13,505– 13,512.

Wengel, C., and Coauthors, 2021: Future high-resolution El Niño/Southern Oscillation dynamics. *Nat. Clim. Chang.* **11**, 758–765.

Willison, J., W. A. Robinson, and G. M. Lackmann, 2013: The Importance of Resolving Mesoscale Latent Heating in the North Atlantic Storm Track. *J. Atmos. Sci.*, **70**, 2234-2250.

Wills, S. M., D. W. J. Thompson, and L. M. Ciasto, 2016: On the Observed Relationships between Variability in Gulf Stream Sea Surface Temperatures and the Atmospheric Circulation over the North Atlantic. *J. Climate*, **29**, 3719-3730.

Wills, S. M., and D. W. J. Thompson, 2018: On the Observed Relationships between Wintertime Variability in Kuroshio–Oyashio Extension Sea Surface Temperatures and the Atmospheric Circulation over the North Pacific. *J. Climate*, **31**, 4669-468.

Wineteer, A., H. S. Torres, and E. Rodriguez, 2020: On the surface current measurement capabilities of spaceborne Doppler scatterometry. *Geophys. Res. Lett*., **47**, e2020GL090116.

Winton, M., S. M. Griffies, B. L. Samuels, J. L. Sarmiento, and T. L. Frölicher, 2013: Connecting Changing Ocean Circulation with Changing Climate. *J. Climate*, **26**, 2268-2278.

Woolf, D. K., 1993: Bubbles and the air-sea transfer velocity of gases. *Atmosphere-Ocean*, **31**, 517–540.

Woollings, T., J. M. Gregory, J. G. Pinto, M. Reyers, and D. J. Brayshaw, 2012: Response of the North Atlantic storm track to climate change shaped by ocean-atmosphere coupling. *Nat. Geosci.*, **5**, 313–317.

Wu., R., B. P. Kirtman, and K. Pegion, 2006: Local Air-Sea Relationship in Observations and Model Simulations. *J. Climate*, **19**, 4914-4932.

Xie, S.-P. 2004: Satellite observations of cool ocean-atmosphere interaction. *Bull. Amer. Meteor. Soc.*, **85**, 195–209.

Xie, T., W. Perrie, and W. Chen, 2010: Gulf Stream thermal fronts detected by synthetic aperture radar. *Geophys. Res. Lett.*, **37**, L06601.

Yang, H., G. Lohmann, W. Wei, M. Dima, M. Ionita, and J. Liu, 2016: Intensification and poleward shift of subtropical western boundary currents in a warming climate. *J. Geophys. Res. Oceans*, **121**, 4928–4945.

Yu, L., 2019: Global air-sea fluxes of heat, fresh water, and momentum: energy budget closure and unanswered questions. *Ann. Rev. Mar. Sci.*, **11**, 227-248.

Zanna, L., P. G. Porta Mana, J. Anstey, T. David, and T. Bolton, 2017: Scale-Aware Deterministic and Stochastic Parametrizations of Eddy-Mean Flow Interaction. *Ocean Modell.*, **111**, 66-80.

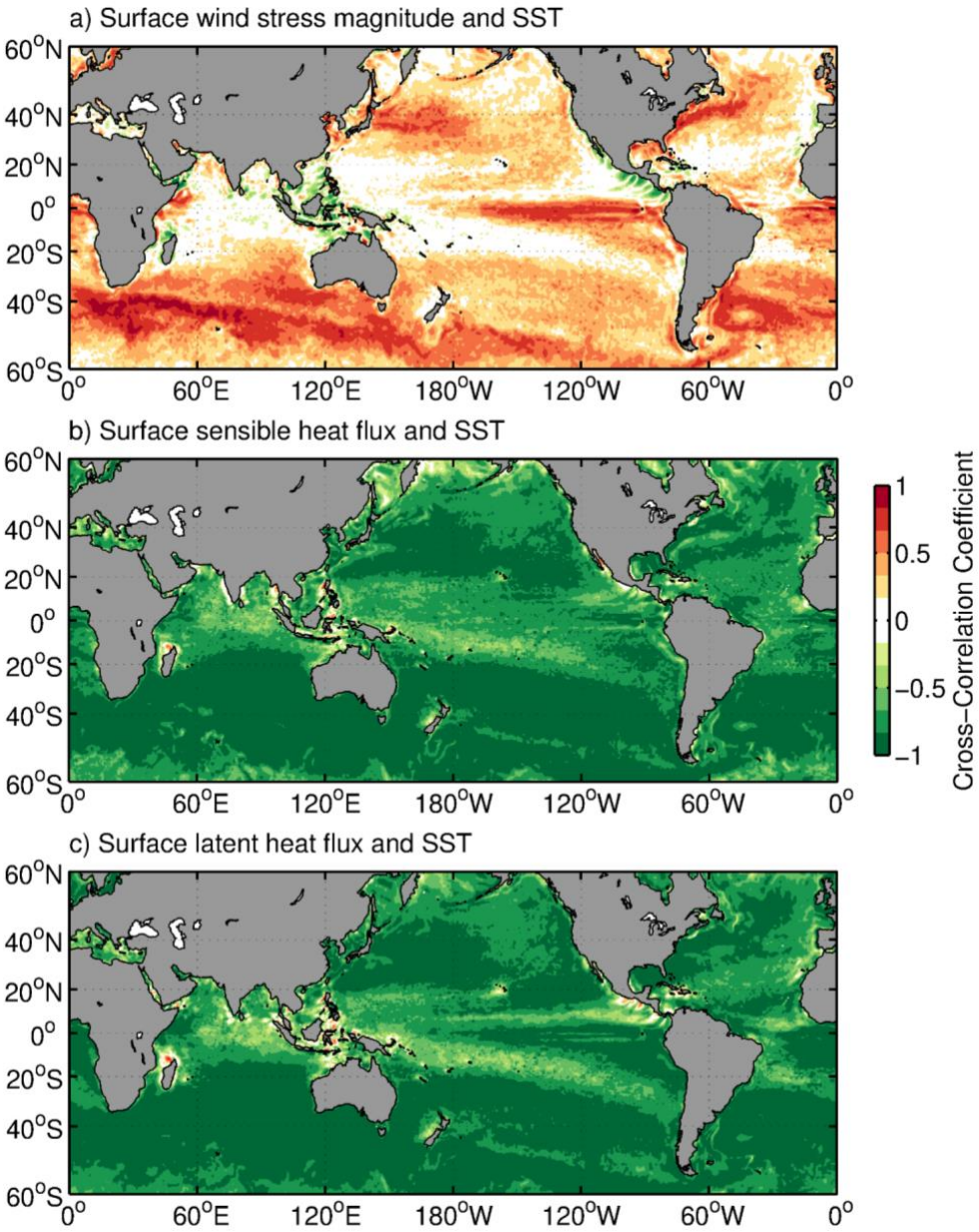

Figure 1: Maps of the cross-correlation coefficients between ERA5 monthly spatially high-pass filtered SST and (a) wind stress magnitude, (b) surface sensible heat flux, and (c) surface latent heat flux. The spatial high-pass filter removed variability with spatial scales greater than 1000 km. The ERA5 reanalysis time period used here was 1991-2020. The standard sign convention for ERA5 surface fluxes is used: positive fluxes mean energy entering into the ocean.

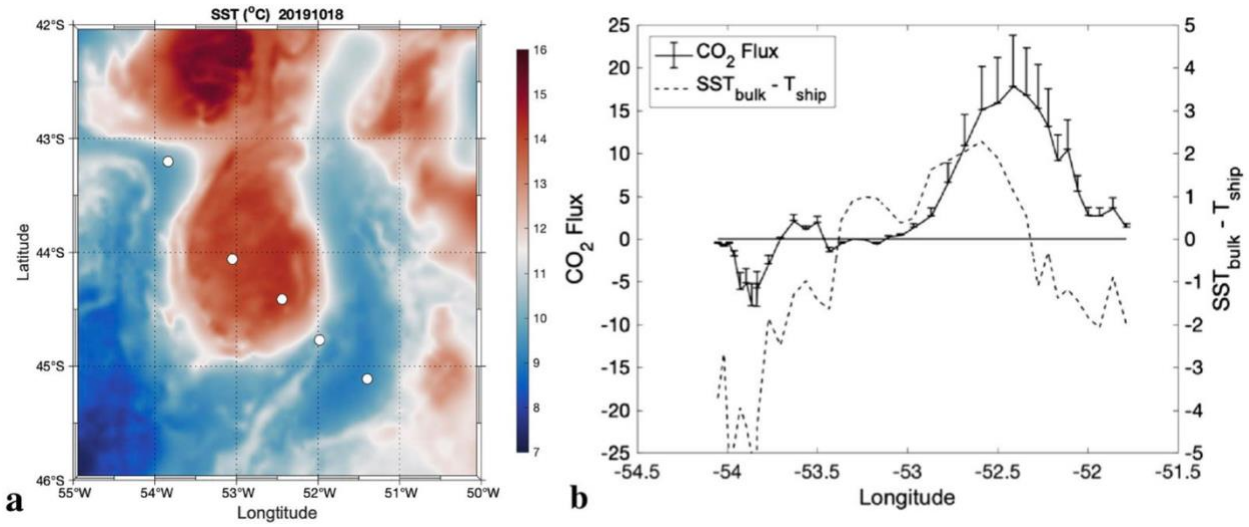

Figure 2: (a) Observed SST (°C) in the Southwestern Atlantic Ocean on 18 October 2019. The white circles denote the Po/V *Almirante Maximiano* trajectory. (b) In situ CO_2 fluxes (μmol $m^{-2}s^{-1}$) measured by Eddy Covariance method (solid) and atmospheric stability parameter SST-Tair (°C) (dotted). The error bars denote the standard error representing a 95% confidence interval. Figures adapted from Pezzi et al. (2021).

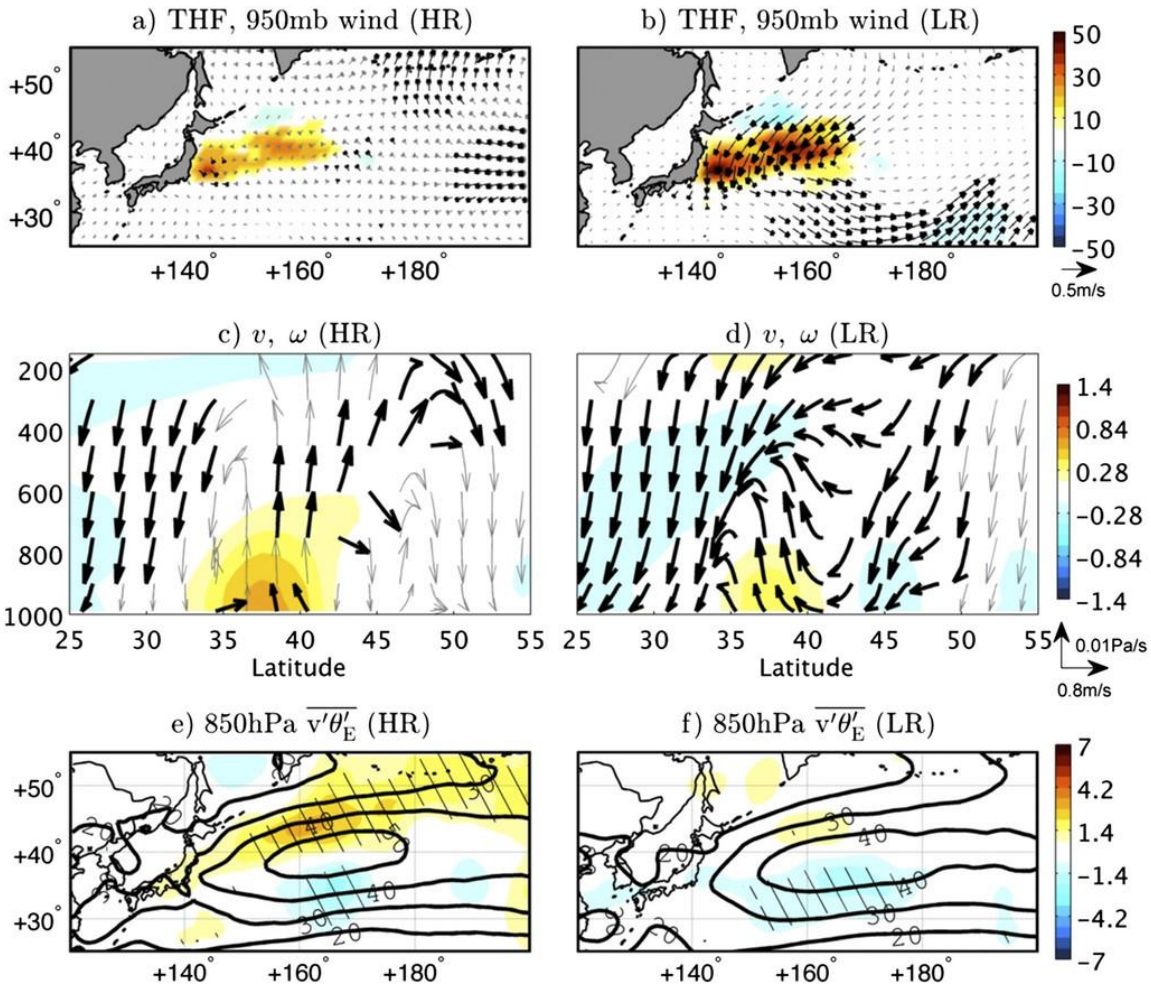

Figure 3: The mean DJF atmospheric response to a shift in the Oyashio Extension SST front in (left) high (¼º) and (right) low (1º) resolution AGCM simulations. (a-b) Turbulent heat flux (colors; Wm^{-2}) and 950-hPa wind (vectors; ms^{-1}). (c-d) Zonally averaged (145–165°E) across-front circulation and equivalent potential temperature (θ_E, colors). (e-f) The 850-hPa poleward energy flux ($\overline{v'\theta_E'}$, colors Kms^{-1}). The black contours indicate climatology. Significant response at 95% confidence level is indicated as thick vectors and stippling. From Smirnov et al. (2015).

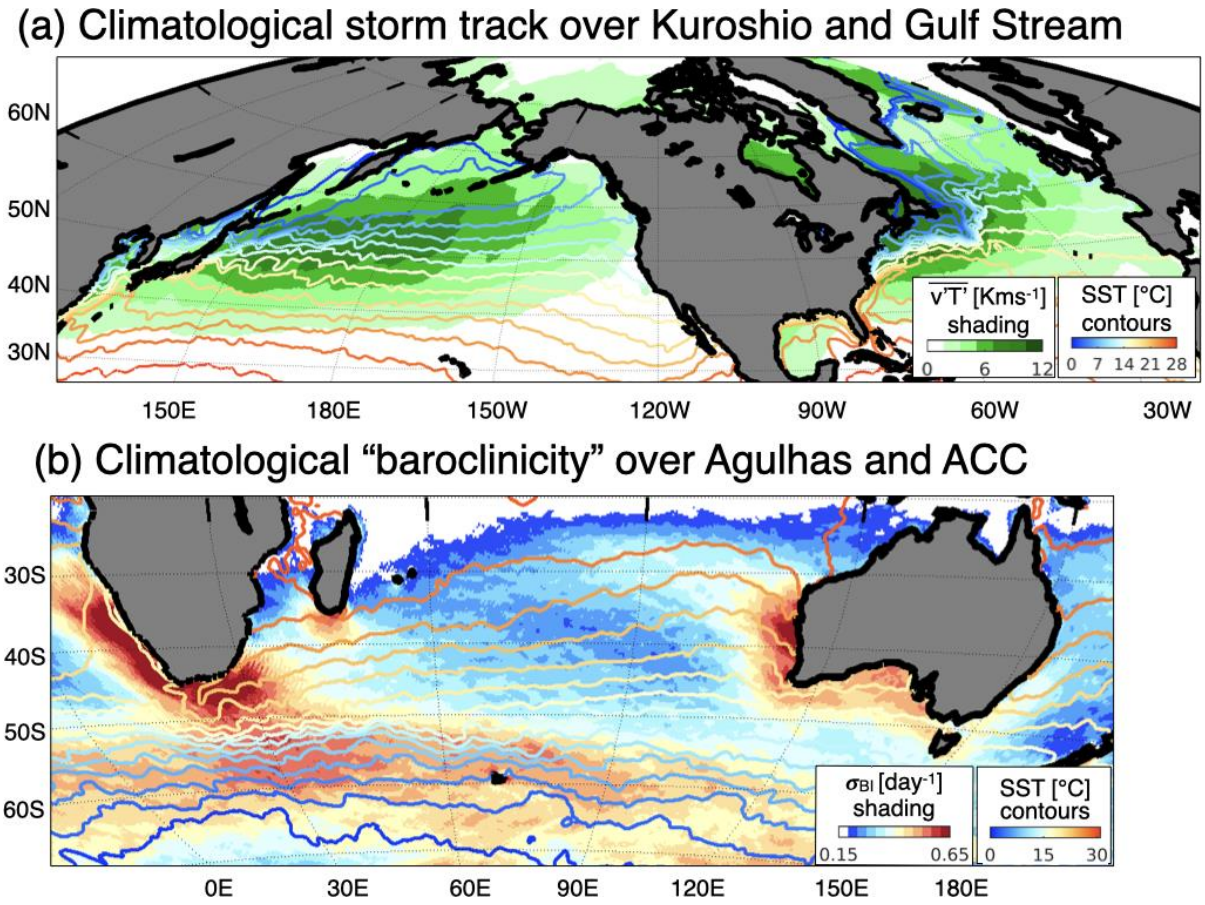

Figure 4: This figure illustrates the climatological relationship of the extratropical storm tracks with the SST fields in (a) Kuroshio-Oyashio Extension and Gulf Stream in the Northern Hemisphere, and (b) Agulhas Current and the Antarctic Circumpolar Current systems in the south Indian Ocean. The atmospheric storm track is estimated in (a) as the time-mean meridional heat transport by transient eddies, $\overline{v'T'}$, at 850 hPa (low troposphere), where primes denote the 2-8-day bandpass filtered fields and the over-bar indicates the time-mean, and in (b) as the maximum Eady growth rate, defined as the most unstable baroclinic mode whose growth rate is scaled as the magnitude of the baroclinicity vector, $|\sigma_{BI}| = 0.31\left(\frac{g}{N\theta}\right)\left|-\frac{\partial\theta}{\partial y}, \frac{\partial\theta}{\partial x}\right|$, at 850 hPa, where g is the gravitational acceleration, N is the buoyancy, and θ is the potential temperature. These storm track quantities are derived from ERA5. The SST climatology is obtained from the NOAA daily Optimum Interpolation dataset. The climatologies are calculated from 2010 to 2015.

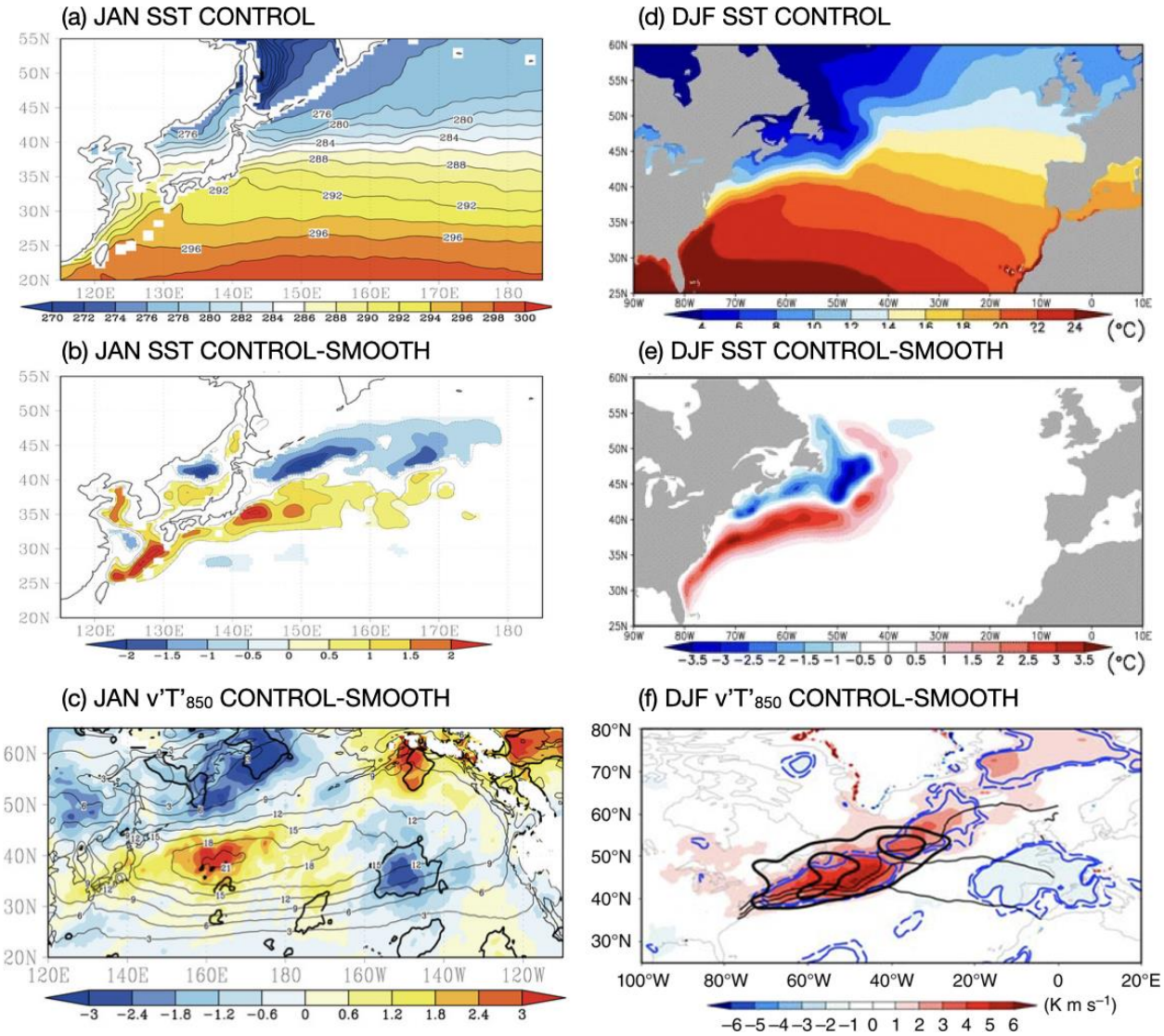

Figure 5: (Left) January observed SST, its difference (CONTROL-SMOOTH), and the difference (CONTROL-SMOOTH) in storm tracks over the North Pacific Ocean. The thin black contours show $\overline{v'T'}$ from the CONTROL case. The 95% confidence level is demonstrated by thick contours. (Right) As in (left) but for over the North Atlantic. Black contours in (f) denote Eady growth rate at 775hPa. The dashed and solid blue contours indicate significant differences at the 10 and 5% levels, respectively. Figures adapted from Kuwano-Yoshida and Minobe (2017) and O'Reilly et al. (2016, 2017).

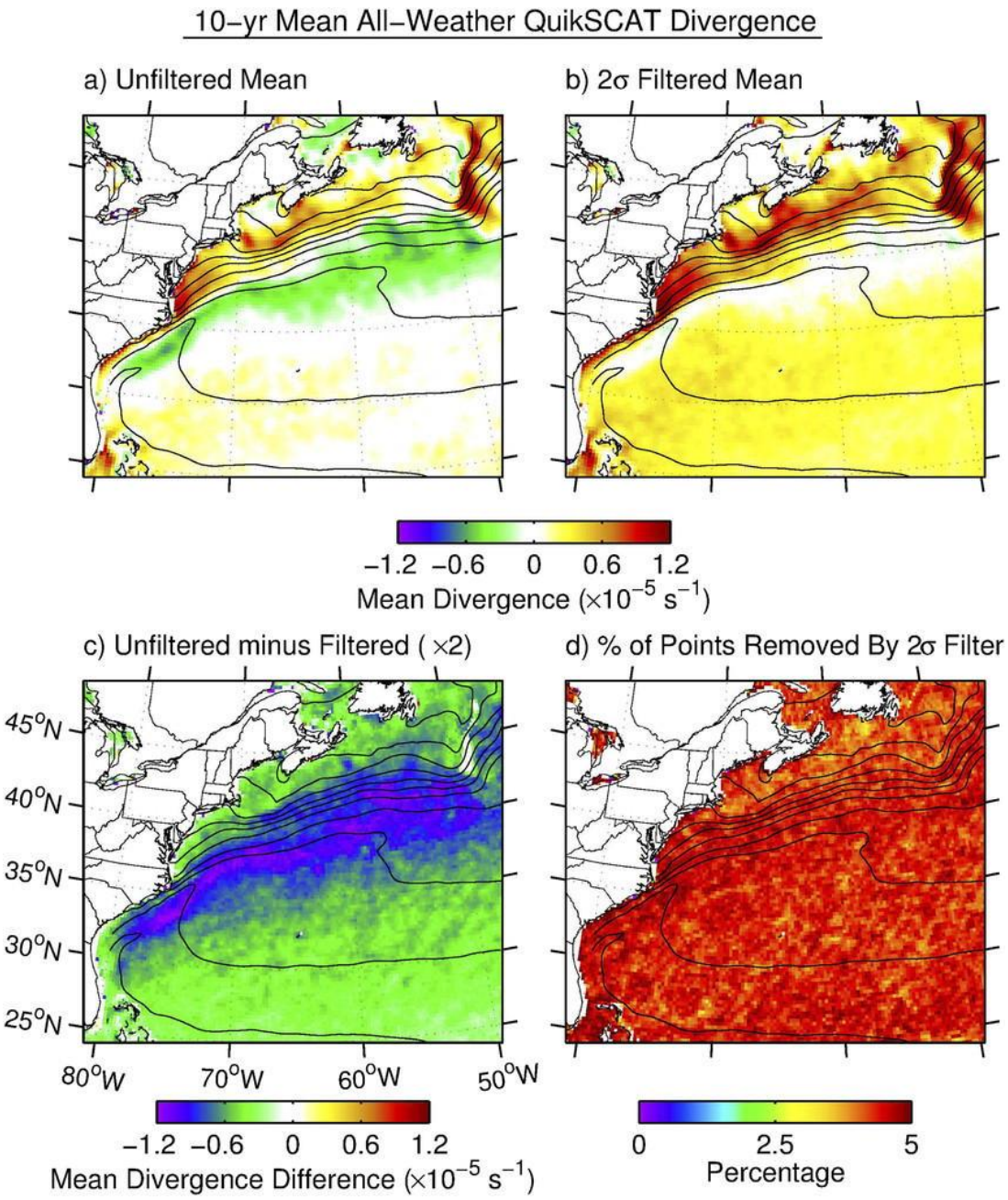

Figure 6: Maps of the 10-yr-mean QuikSCAT all-weather divergence (a) consisting of all points; (b) after application of the 2σ temporal extreme-value filter; (c) difference between (a) and (b); and (d) the percentage of divergence points removed by the 2σ extreme-value filter. The contours in each panel are of the 10-yr-mean Reynolds SST with a contour interval of 2ºC. From O'Neill et al. (2017).

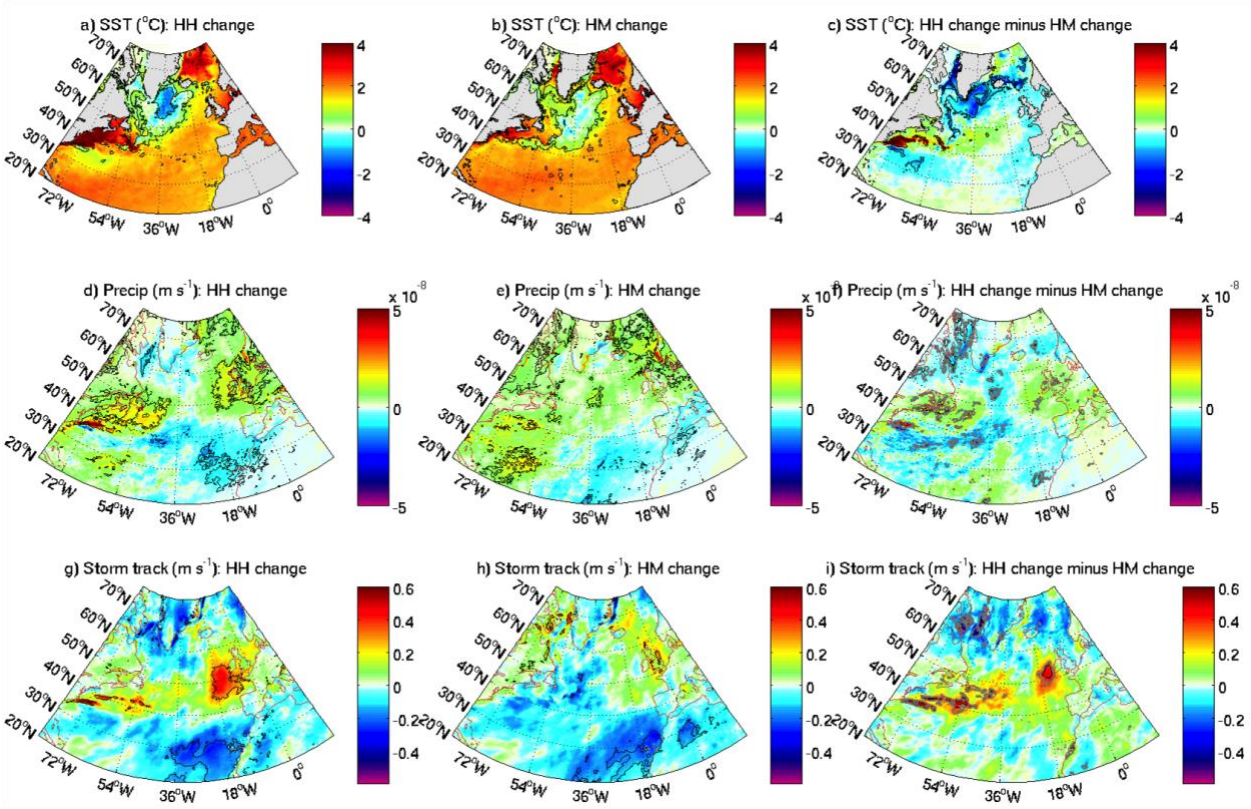

Figure 7: (a-c) 2031–2050 minus 1951–1970 differences simulated by the HadGEM3-GC3.1, with 25 km atmospheric resolution coupled to 1/4° ocean (eddy-permitting, HM) and 1/12° ocean (eddy-rich, HH): SST (°C) (a) HH and (b) HM, precipitation (ms^{-1}) (d) HH and (e) HM; surface storm track (ms^{-1}) (g) HH and (h) HM. Panels (c, f, i) show the difference between the HH future change and the HM change. The black lines denote the 95% significance. Gray lines in (c,f,i) denote the 90% significance. From Grist et al. (2021).

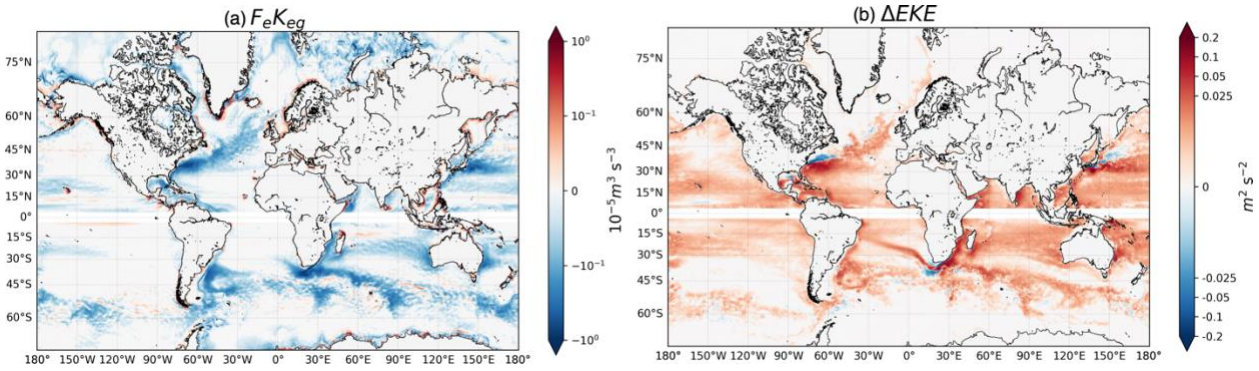

Figure 8: (a) Geostrophic eddy wind work (10^{-5} m^3s^{-3}) estimated from the EC-Earth global coupled simulation with current feedback (CFB). The negative values indicate a transfer of momentum from geostrophic mesoscale currents to the atmosphere. This sink of energy is the main driver of the damping of EKE illustrated in (b), as illustrated by the difference of EKE (m^2 s^{-2}) between simulations without CFB and with CFB. Both wind work and EKE are estimated over a 30-yr. period. Details about the coupled model and experiments can be found in Renault et al. (unpublished manuscript).

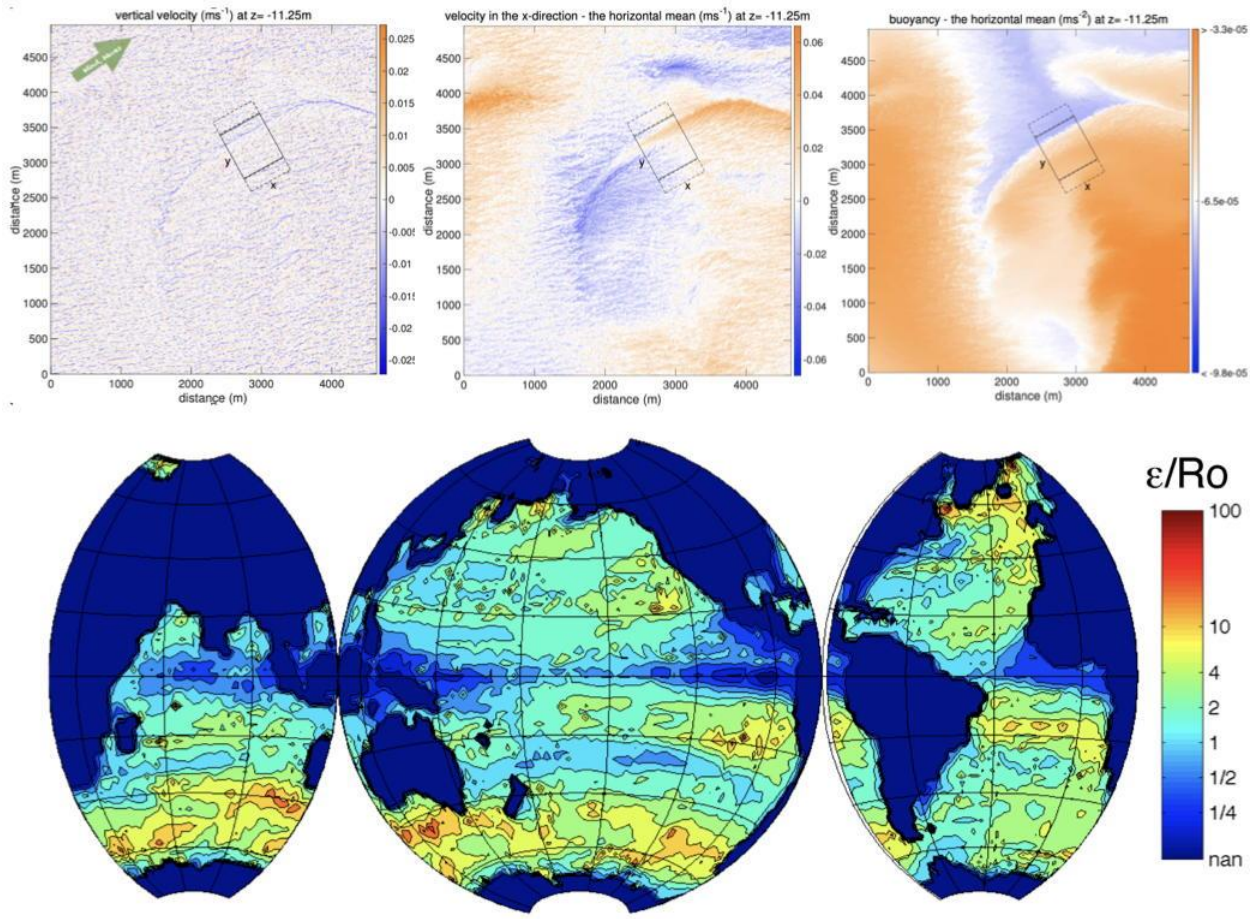

Figure 9: (Upper panel) Examples of a front interacting with Langmuir turbulence (box centered on this feature), which is aligned in the downwind and down-Stokes direction. (Left) vertical velocity showing ubiquitous Langmuir cells, but also a long, coherent (downwelling) overturning circulation along the front due to frontogenesis and accelerated by the Stokes shear force. (Center) Along-front (x-direction) velocity shows the frontal flow. (Right) The front is characterized by a sharp transition in buoyancy (or temperature). Adapted from Suzuki et al. (2016). (lower panel) Estimated ratio of ε (strength of Stokes drift-induced vertical acceleration vs. buoyancy, an indicator of wave contributions added to the traditional hydrostatic balance) to Rossby number (indicating geostrophic balance). This ratio implies the deviation from hydrostatic balance due to waves as compared to the deviation from geostrophic balance due to advection. This estimate is based on the de Boyer-Montegut et al. (2004) mixed layer depth climatology (h) and a global simulation of WaveWatch3, and AVISO geostrophic velocity. Figures redrawn from McWilliams and Fox-Kemper (2013).

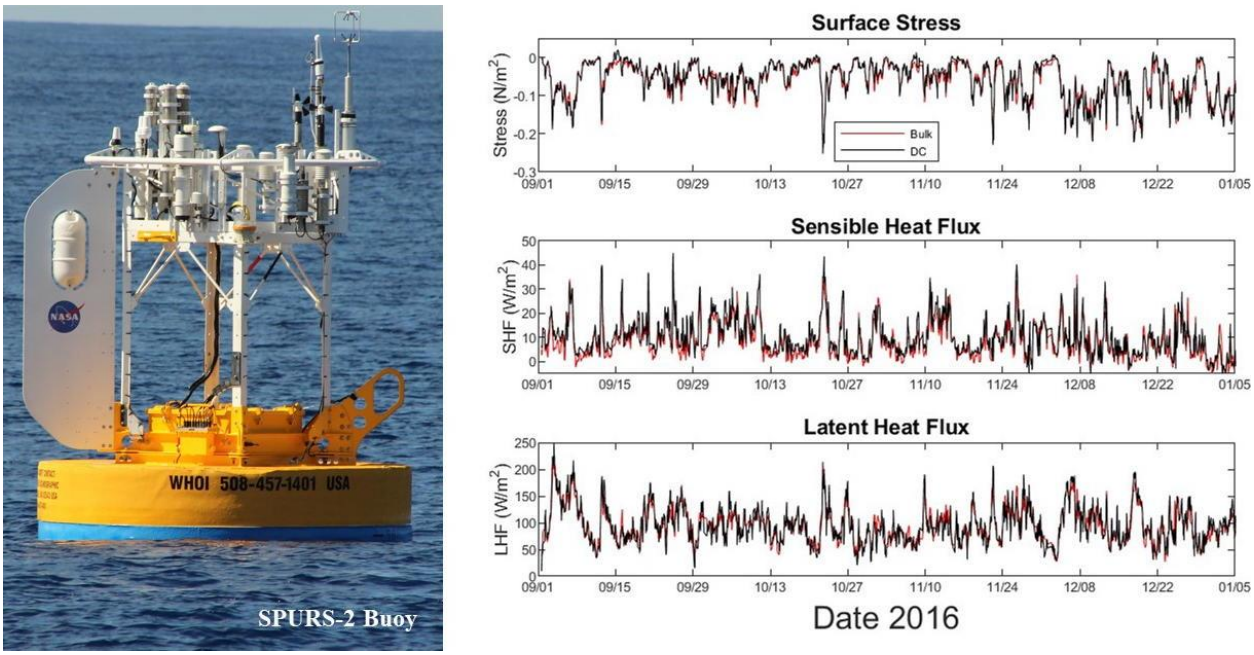

Figure 10: (left) The SPURS-2 central mooring with instrumentation at the upper right includes a sonic anemometer, infrared hygrometer, and sensors to remove buoy motion. The sensor package can directly measure the surface stress, sensible heat, and latent heat fluxes. (right) Time series of these fluxes showing bulk estimates in red and direct covariance (DC) fluxes in black. Good agreement is seen between the bulk and DC estimates, with the most significant discrepancies visible in the sensible heat flux. Photo by James B. Edson (WHOI).